Hierarchical neural architecture underlying thirst regulation

Vineet Augustine[1,2], **Sertan Kutal Gokce**[#2], **Sangjun Lee**[#2], **Bo Wang**[2], **Thomas J. Davidson**[3], **Frank Reimann**[4], **Fiona Gribble**[4], **Karl Deisseroth**[5,6], **Carlos Lois**[2], and **Yuki Oka**[1,2]

[1]Computation and Neural Systems, California Institute of Technology, Pasadena, California, USA

[2]Division of Biology and Biological Engineering, California Institute of Technology, Pasadena, California, USA

[3]Department of Physiology and Kavli Institute for Fundamental Neuroscience, University of California, San Francisco, California, USA

[4]Department of Clinical Biochemistry, University of Cambridge, Cambridge, UK

[5]Howard Hughes Medical Institute, Stanford University, Stanford, California, USA.

[6]Department of Bioengineering, Stanford University, Stanford, California, USA.

[#] These authors contributed equally to this work.

Abstract

Neural circuits for appetites are regulated by both homeostatic perturbations and ingestive behaviour. However, the circuit organization that integrates these internal and external stimuli is unclear. Here we show in mice that excitatory neural populations in the lamina terminalis form a hierarchical circuit architecture to regulate thirst. Among them, nitric oxide synthase-expressing neurons in the median preoptic nucleus (MnPO) are essential for the integration of signals from the thirst-driving neurons of the subfornical organ (SFO). Conversely, a distinct inhibitory circuit, involving MnPO GABAergic neurons that express glucagon-like peptide 1 receptor (GLP1R), is activated immediately upon drinking and monosynaptically inhibits SFO thirst neurons. These responses are induced by the ingestion of fluids but not solids, and are time-locked to the onset and offset of drinking. Furthermore, loss-of-function manipulations of GLP1R-expressing MnPO neurons lead to a polydipsic, overdrinking phenotype. These neurons therefore facilitate rapid

satiety of thirst by monitoring real-time fluid ingestion. Our study reveals dynamic thirst circuits that integrate the homeostatic-instinctive requirement for fluids and the consequent drinking behaviour to maintain internal water balance.

The precise regulation of water intake is critical to the maintenance of fluid homeostasis in the body. The initiation of drinking in animals is triggered by internal fluid imbalance, such as water depletion[1–4]. By contrast, drinking is terminated rapidly when animals have ingested a sufficient amount of water, which generally precedes the absorption of the ingested fluid[5–10]. To achieve such accurate fluid regulation, the brain needs to monitor both internal water balance and fluid ingestion on a real-time basis[11,12]. How the brain integrates homeostatic and behavioural inputs to coordinate drinking behaviour is an unsolved question. As such, uncovering the neural circuits that process these regulatory signals is a critical step in understanding the neural logic of thirst regulation[13–15].

The lamina terminalis is the principal brain structure responsible for sensing and regulating internal water balance[3,5,16,17]. It contains three main nuclei: the SFO, the organum vasculosum lamina terminalis (OVLT) and the MnPO, all of which are anatomically inter-connected[17–21]. The SFO and the OVLT in particular are two major osmosensory sites in the brain because they lack the normal blood-brain barrier. Recent studies have shown that specific neural populations in the lamina terminalis have a causal role in the regulation of drinking behaviour. For instance, optogenetic and chemogenetic activation of excitatory SFO neurons co-expressing a transcription factor, ETV1, and nitric oxide synthase (SFO^{nNOS} neurons) drives immediate and robust drinking behaviour[19,22,23]. Conversely, stimulation of inhibitory populations of lamina terminalis nuclei suppresses water intake[19,24]. Although these studies pinpointed the neural substrates that regulate thirst, the circuit organization that mediates drinking behaviour remains poorly understood, owing to anatomical complexity and the lack of genetic handles.

Here we focused on the neural architecture of the lamina terminalis, and investigated genetically defined thirst circuits using neural manipulation, tracing and *in vivo* optical recording approaches.

Hierarchical circuit for thirst

SFO^{nNOS} neurons project their axons to other nuclei of the lamina terminalis (OVLT and MnPO)[10,25], as well as to the paraventricular and supraoptic nuclei, which contain vasopressin-expressing neurons[19]. These axonal projections and the downstream neurons define a framework of circuit elements that control thirst-related behaviours and hormonal outputs[26]. To identify genetically defined SFO^{nNOS} downstream populations that regulate drinking, we used optogenetics along with monosynaptic rabies tracing. Water restriction induces robust c-Fos expression in the SFO and putative downstream regions (Extended Data Fig. 1a). In the MnPO and OVLT, essentially all of the c-Fos signals were found in nNOS-expressing excitatory neurons (MnPO^{nNOS} and OVLT^{nNOS}; Extended Data Fig. 1a, top, b). Similar results were obtained when we photostimulated SFO^{nNOS} neurons by expressing channelrhodopsin (ChR2)[27] using adeno-associated virus (AAV-DIO-ChR2) in *nNOS-cre* (also known as *Nos1-cre)* mice (Extended Data Fig. 1a, bottom). These data

suggest that MnPO^{nNOS} and OVLT^{nNOS} neurons are putative downstream populations of SFO^{nNOS} neurons. Retrograde monosynaptic rabies tracing[28] from MnPO^{nNOS} and OVLT^{nNOS} neurons confirmed direct connections with the SFO^{nNOS} population (Fig. 1a, b and Extended Data Fig. 1c). Moreover, photostimulation of ChR2-expressing MnPO^{nNOS} or OVLT^{nNOS} neurons selectively induced water drinking in satiated mice (Extended Data Fig. 1d). These studies demonstrated that SFO^{nNOS} neurons send monosynaptic excitatory inputs to the MnPO^{nNOS} and OVLT^{nNOS} populations, each of which is sufficient to trigger water drinking.

To further investigate the circuit architecture that processes the internal need for water, we performed neural epistasis analysis for the circuits of the lamina terminalis by loss-of-function manipulation (Fig. 1c). We reasoned that if SFO^{nNOS} and its downstream populations redundantly encode thirst in parallel, the ablation of one population should have only minor effects on drinking. Alternatively, if the circuit is organized in a hierarchical fashion in which a specific population has a critical role, the elimination of such a downstream population should abolish SFO^{nNOS}-stimulated drinking. To test these ideas, we expressed caspase (AAV-flex-Casp3)[29] in the MnPO, OVLT or SFO of *nNOS-cre* mice (Fig. 1c). The expression of Casp3 resulted in the specific and near-complete elimination of nNOS-expressing neurons of a given nucleus (Fig. 1d and Extended Data Fig. 2a). In OVLT^{nNOS}-ablated and control mice, photostimulation of SFO^{nNOS} neurons triggered robust drinking (Fig. 1e and Extended Data Fig. 2b). By sharp contrast, the ablation of MnPO^{nNOS} neurons markedly suppressed SFO^{nNOS}-stimulated water intake (Fig. 1e and Extended Data Fig. 2b, MnPOx). We also found that MnPO^{nNOS} neurons have an important role in the drinking behaviour evoked by OVLT^{nNOS} neurons. Water intake induced by photostimulation of OVLT^{nNOS} neurons was significantly attenuated after ablating MnPO^{nNOS}, but not SFO^{nNOS} neurons (Extended Data Fig. 2c). These results suggest that MnPO^{nNOS} neurons are essential neural substrates of the lamina terminalis for the behavioural output. If this model is correct, stimulating the MnPO^{nNOS} population without the inputs from their upstream SFO^{nNOS}, or both SFO^{nNOS} and OVLT^{nNOS}, neurons should still trigger robust drinking (Fig. 1c). As hypothesized, the elimination of these populations had no impact on drinking when MnPO^{nNOS} neurons were directly photostimulated (Fig. 1e and Extended Data Fig. 2b, SFOx, SFOx and OVLTx). Similar results were obtained by chemogenetic acute silencing using hM4Di (ref. 30) (Fig. 1f). In awake mice, acute inhibition of MnPO^{nNOS} neurons by clozapine N-oxide (CNO) severely suppressed water consumption in both water-restricted and SFO^{nNOS}-stimulated mice (Fig. 1g and Extended Data Fig. 2d, e). However, the same manipulation did not decrease sugar consumption in food-restricted mice (Fig. 1g and Extended Data Fig. 2d, e).

Importantly, the silencing of MnPO^{nNOS} neurons did not compromise the osmosensory function of the SFO^{nNOS} population. We used fibre photometry[31] in awake-behaving mice that expressed the calcium indicator GCaMP6s in the SFO^{nNOS}, and the neuronal silencer hM4Di in MnPO^{nNOS} neurons (Fig. 1h). We showed that the activation of SFO^{nNOS} neurons by osmotic stress was unaffected in the absence of functioning MnPO^{nNOS} neurons (Fig. 1i and Extended Data Fig. 2f). These results were supported by our electrophysiological recordings: only a minor fraction of SFO neurons received monosynaptic input from MnPO^{nNOS} neurons (Extended Data Fig. 3), demonstrating the unidirectional connection

from SFO[nNOS] to MnPO[nNOS] neurons. Taken together, our results demonstrate that thirst neurons in the lamina terminalis form a hierarchical circuit organization, and that the MnPO[nNOS] population is required to process signals from SFO[nNOS] neurons to coordinate drinking.

MnPO[GLP1R] → SFO[nNOS] inhibitory input

The thirst neurons of the lamina terminalis also receive negative feedback regulation upon drinking itself[1,8,10]. It has been shown that water intake rapidly suppresses the activity of thirst neurons in the lamina terminalis[10,18] (Extended Data Fig. 4). It is suggested that this quick regulation of thirst circuits optimizes fluid ingestion[8,9]. To examine the neural basis of drinking-induced thirst inhibition, we functionally mapped the upstream inhibitory circuits of SFO[nNOS] neurons using two neural tracing approaches. First, we retrogradely labelled inhibitory neurons that project to the SFO by injecting herpes simplex virus conjugated with mCherry (HSV-mCherry) into the SFO of *Vgat-cre* mice (Fig. 2a, left). Among the putative upstream structures (Extended Data Fig. 5a), the MnPO contained the strongest HSV signals (Fig. 2a, right). Next, we performed monosynaptic rabies tracing from SFO[nNOS] neurons (Extended Data Fig. 5b). Consistent with the results of the HSV tracing, the MnPO contained the greatest number of rabies-virus-positive neurons that minimally overlapped with excitatory neurons (Extended Data Fig. 5b). These complementary tracing results suggest that GABAergic neurons in the MnPO are a major source of inhibitory input to the SFO[24].

To gain a more specific genetic handle on these neurons, we performed RNA sequencing analysis of the inhibitory population of the dorsal lamina terminalis (containing the MnPO and SFO) and the cortex. We found that GLP1R transcripts were highly enriched in the inhibitory neurons from the lamina terminalis, by a factor of 100 compared to the cortex (Fig. 2b). *In situ* hybridization and immunohistochemical studies in *Glp1r-cre* mice[32] confirmed that GABAergic MnPO neurons expressed GLP1R (Fig. 2c and Extended Data Fig. 6a, b). As predicted from our tracing results, ChR2-assisted circuit mapping[33] revealed that all recorded SFO[nNOS] neurons (16 out of 16 cells) received robust monosynaptic inhibitory input from GLP1R-expressing MnPO (MnPO[GLP1R]) neurons, with an inhibitory postsynaptic current latency of 8.4 ms (Fig. 2d). However, SFO[non-nNOS] neurons received such input rarely (4 out of 15 cells with small inhibitory postsynaptic currents, Fig. 2d), showing that inhibitory input from MnPO[GLP1R] neurons is specific to excitatory neurons in the SFO. Furthermore, photostimulation of MnPO[GLP1R] neurons selectively suppressed water intake in thirsty mice (Fig. 2e and Extended Data Fig. 6c), although this acute inhibition was not observed upon the application of a GLP1R agonist[34] (Extended Data Fig. 6d–f). Collectively, our findings suggest that the MnPO[GLP1R] population has a key modulatory role in thirst.

MnPO[GLP1R] neurons monitor liquid intake

Next, we measured the *in vivo* calcium dynamics of MnPO[GLP1R] neurons expressing GCaMP6s in *Glp1r-cre* mice (Fig. 3a). In freely moving mice, MnPO[GLP1R] neurons were acutely activated during water drinking, and their activity returned to the basal level when

they stopped drinking (Fig. 3a, red trace). These neurons responded equally when thirsty mice licked either water or isotonic saline, but not when they licked an empty spout (Fig. 3b and Extended Data Fig. 7c–e). Notably, the neuronal responses were also observed when the mice licked non-aqueous silicone oil, which showed that the activation of MnPO^{GLP1R} neurons is independent of fluid composition. Under food-restricted conditions, we found that MnPO^{GLP1R} neurons still responded upon licking sucrose solution (300 mM, Fig. 3c and Extended Data Fig. 7c, d). However, solid peanut butter evoked no response despite its high palatability (Fig. 3c). These optical recording studies indicate that MnPO^{GLP1R} neurons are activated purely by fluid consumption and not by reward-seeking behaviour or licking action per se. Consistent with the connection from MnPO^{GLP1R} to SFO^{nNOS} neurons, the activity of the SFO^{nNOS} population mirrored precisely the calcium dynamics of MnPO^{GLP1R} neurons, except that water intake evoked an additional persistent inhibition (Extended Data Fig. 7a, b). This water-specific inhibition of SFO^{nNOS} neurons is probably due to osmolality sensing or water absorption in the gastrointestinal tract as proposed previously[1,9]. These results demonstrate two important properties of thirst circuits. First, MnPO^{GLP1R} neurons are activated upon fluid ingestion; this activation is independent of fluid composition and the internal state of the animal. Second, this neural population transmits inhibitory signals to SFO^{nNOS} neurons, in a manner that is time-locked to drinking.

Effect of eating and drinking

We investigated the mechanisms by which MnPO^{GLP1R} neurons exclusively represent fluid intake. To this end, we provided water-restricted mice with water in two different forms— liquid and gel (HydroGel: 98% water + hydrocolloids)—while recording MnPO^{GLP1R} activity (Fig. 4a). In either form, the mice ingested a similar amount of water within the 30-min session (Fig. 4b). Notably, compared to the robust activation of MnPO^{GLP1R} neurons upon drinking water, gel-eating behaviour did not elicit any response (Fig. 4a, c). Similarly, eating normal chow did not stimulate this neural population (Fig. 4d). Therefore, MnPO^{GLP1R} neurons are able to distinguish between drinking and eating behaviour even if an animal consumes essentially the same substance. These results suggest that the MnPO^{GLP1R} population facilitates satiety, which is induced by drinking behavior and not specifically by water.

Because the rate of ingestion differed considerably between the drinking of water and the eating of HydroGel (Fig. 4b), we speculated that MnPO^{GLP1R} neurons may monitor the pattern of ingestion in order to distinguish the mode of consumption. To examine this possibility, mice were given access to water for 30 s in total at two different rates: 2 s $\times$ 15 times and 30 s $\times$ 1 time (Fig. 4e). As hypothesized, concentrated periods of drinking evoked significantly greater responses in the MnPO^{GLP1R} neurons than did sparse periods of drinking, regardless of the total amount of water consumed (Fig. 4e). We note that the temperature of the fluid did not affect the response (Fig. 4f). Because animals can ingest fluids much faster than they can ingest solid substances, these data strongly support the idea that the MnPO^{GLP1R} population distinguishes between drinking and eating on the basis of ingestion speed. Consequently, concentrated (that is, rapid) fluid intake recruits MnPO^{GLP1R}-mediated inhibition signals, which in turn suppress the activity of SFO^{nNOS}

neurons. These findings provide key mechanistic insight into rapid thirst alleviation as a result of drinking behaviour.

MnPO^{GLP1R} neurons help thirst satiety

In view of the function of the MnPO^{GLP1R} population in the monitoring of fluid intake, we next considered its physiological importance in the regulation of drinking using chemogenetic loss-of-function manipulation (Fig. 5a). Whereas any fluid elicits transient MnPO^{GLP1R}→ SFO^{nNOS} inhibition, water evokes an additional inhibitory effect that persists after drinking episodes (Extended Data Fig. 7a). Owing to this water-specific signal, inhibition of MnPO^{GLP1R} neurons by CNO had only a minor effect on the total water intake of water-restricted mice during a 30-minute period (Extended Data Fig. 8a, b, d). By contrast, marked effects were observed for isotonic saline, in which MnPO^{GLP1R}-independent inhibitory signals are absent (Fig. 5b). Compared to the vehicle control, inhibition of MnPO^{GLP1R} neurons robustly increased both the total amount and the duration of saline intake (Fig. 5c and Extended Data Fig. 8c). However, under satiated conditions, the same manipulation did not increase water or saline intake, which excludes the possibility that inhibiting MnPO^{GLP1R} neurons stimulates appetite directly (Fig. 5c). We observed the same overdrinking phenotype in mice in which MnPO^{GLP1R} neurons were ablated by Casp3 (Extended Data Fig. 8e, f). Our functional manipulation studies demonstrate that MnPO^{GLP1R} neurons promote satiety of thirst by monitoring real-time fluid intake, and that the malfunction of this neuronal regulation leads to polydipsic overdrinking, especially in the case of non-hypoosmotic fluids such as saline.

Discussion

In this study, we identified genetically defined thirst circuits in the lamina terminalis that integrate the instinctive need for water with the consequent drinking behaviour to maintain internal water balance (Fig. 5d). We showed that multiple downstream populations of SFO^{nNOS} neurons are individually sufficient to induce water intake. These data are reminiscent of the circuit organization for hunger, in which eating behaviour is redundantly encoded by multiple output projections of AgRP neurons in the arcuate nucleus[35]. However, we showed that individual thirst-related neuronal populations of the lamina terminalis are hierarchically organized, and that MnPO^{nNOS} neurons are the behavioural output neurons. Previous lesion studies in rats and sheep have proposed a model in which the MnPO serves as a critical site that integrates inputs from osmosensory neurons of the SFO and the OVLT[36]–[38]. Our findings well explain and further advance the concept of this model with cell-type-specific precision. Whereas the necessity of the SFO may vary among species[10], the MnPO appears to consistently function as the key centre for drinking across species[38]. In our analysis, MnPO^{nNOS} neurons project to various areas including the hypothalamus and the midbrain (Extended Data Fig. 9a; see also ref. 18). These results reveal a neural logic to thirst processing in the lamina terminalis circuit, and provide a platform for investigation into how the appetite for water is integrated at downstream sites of MnPO^{nNOS} neurons.

Notably, MnPO^{GLP1R} neurons responded selectively to the ingestion of fluids but not solids. These inhibitory neurons provide rapid monosynaptic inhibition to thirst-driving SFO^{nNOS}

neurons. Our results indicate strongly that the MnPO^{GLP1R} population facilitates thirst satiation upon drinking rather than upon water absorption. At a psychophysical level, these findings provide an explanation for the long-standing observation that thirst is quickly alleviated at the onset of drinking[6,9]. At a physiological level, these results reveal a neural interface that adjusts the activity of thirst neurons on the basis of real-time drinking behaviour. Although systemic recovery of fluid balance relies on water absorption into the blood, thirst is modulated by multiple preabsorptive factors including oral, oropharyngeal and gastrointestinal signals[1]. It is unlikely that the MnPO$^{GLP1R} \rightarrow$ SFO^{nNOS} circuit mediates oral sensory information such as taste[39–41] because it responds to any fluid, including silicone oil. Instead, MnPO^{GLP1R} neurons may function as a flow-meter by sensing gulping actions in the oropharyngeal area, and provide rapid, liquid-specific inhibition to thirst circuits. This idea is consistent with previous findings that drinking hyperosmotic saline[7], but not eating food[42], transiently suppressed vasopressin secretion. In this model, MnPO^{GLP1R} neurons serve as a central detector that discriminates fluid ingestion from solid ingestion, which promotes acute satiation of thirst through the SFO and other downstream targets (Extended Data Fig. 9b). Subsequently, gastrointestinal mechanisms may selectively detect water over other fluids that induce persistent inhibitory effects on SFO^{nNOS} neurons (Extended Data Fig. 7a). Although fluid-sensing mechanisms at each peripheral area are poorly understood, further molecular and cellular studies should help to reveal complex regulatory signals that maintain body-fluid homeostasis.

METHODS

Animals.

All animal procedures were performed in accordance with the US NIH guidance for the care and use of laboratory animals and were approved by the Institutional Animal Care and Use Committee (protocol no: 1694-14, California Institute of Technology). Mice used for data collection were both males and females, at least eight weeks of age. The following mice were purchased from the Jackson Laboratory: C57BL/6J, stock number 000664; *Slc32a1-cre* (also known as *Vgat-cre*), stock number 016962; Ai9, stock number 007909; Ai3, stock number 007903; *Slc17a6-cre* (also known as *Vglut2-cre*), stock number 016963 and *Nos1-cre*, stock number 017526. *Glp1r-cre* and Ai110 lines were provided by F. Gribble (Cambridge) and D. Anderson (Caltech), respectively. Mice were housed in temperature- and humidity-controlled rooms with a 13 h:11 h light:dark cycle with *ad libitum* access to chow and water.

Viral constructs.

The following AAVs were purchased from the UNC Vector Core: AAV1-CA-FLEX-RG, 4×10^{12} copies per ml; AAV1-EF1a-FLEX-TVA-mCherry, 6×10^{12} copies per ml; AAV2-EF1a-DIO-hChR2-eYFP, 5.6×10^{12} copies per ml; AAV2-hSyn-DIO-hM4D(Gi)-mCherry, 3.7×10^{12} copies per ml; AAV2-EF1a-DIO-mCherry, 5.7×10^{12} copies per ml; AAV5-CamKIIa-hM4D(Gi)-mCherry, 4.3×10^{12} copies per ml; AAV5-CamKIIa-hM3D(Gq)-mCherry, 1.7×10^{12} copies per ml; AAV5-FLEX-taCasp3-TEVp, 5.3×10^{12} copies per ml. The following AAVs were purchased from the UPenn Vector Core: AAV1-Syn-FLEX-GCaMP6s-WPRE-SV40, 2.9×10^{13} genome copies per ml; AAV1-Syn-GCaMP6s-WPRE-

SV40, 2.28×10^{13} genome copies per ml; AAV1-CamKII-eYFP-WPRE-hGH, 1.86×10^{13} genome copies per ml; AAV2-EF1a-DIO-eYFP-WPRE-hGH, 3.05×10^{12} genome copies per ml. EnvA G-deleted Rabies-eGFP (1.6×10^8 transduction units per ml) was purchased from the Salk Institute. Herpes simplex virus (hEF1a-LS1L-mCherry HT) was purchased from the Vector Core Facility at the Massachusetts Institute of Technology.

Surgery.

All procedures were adopted from a previous report[19]. Mice were anaesthetized with a mixture of ketamine (1 mg ml^{-1}) and xylazine (10 mg ml^{-1}) in isotonic saline, injected intraperitoneally (i.p.) at 10 µl g^{-1} bodyweight. The mice were then placed in a stereotaxic apparatus (Narishige Apparatus) on a heating pad. An incision was made to expose the skull. The three-dimensional magnetic resonance imaging coordinate system was used to align the skull reference. A small craniotomy, less than 1 mm, was made using a hand drill at the regions of interest. Viral constructs were injected using a pressure injection system (Nanoliter 2000) using a pulled glass capillary at 100 nl min^{-1}. The coordinates were: anteroposterior −4,030, mediolateral 0, dorsoventral −2,550 (200-nl injection) for the SFO; anteroposterior −3,100, mediolateral 0, dorsoventral −4,080 (100-nl injection) and −3,800 (50–100-nl injection) for the MnPO; and anteroposterior −2,700, mediolateral 0, dorsoventral −4,900 (75-nl injection) for the OVLT. For optogenetic implants, a 200-µm fibre bundle (FT200EMT, Thorlabs) glued to a ceramic ferrule (Thorlabs) with epoxy was used. For photometry implants, a 400-µm fibre bundle (BFH48-400, Thorlabs) glued to a ceramic ferrule with low autofluorescence epoxy (EPO-TEK301) or a custom-made implant (Doric Lenses) was used. A fibre was implanted 200–300 µm (for photostimulation) or 0–50 µm (for photometry) above the virus injection site. After the application of a local anaesthetic to the sides of the skin incision, the implants were permanently fixed to the skull using dental cement. Cannulated mice were placed in a clean cage on a heating pad to recover from anaesthesia. Mice were kept in their home cage for at least ten days before any behavioural tests.

Photostimulation.

For optogenetic experiments, photostimulation was performed using 473-nm laser pulses: 20 ms, 5 Hz (for OVLT) or 20 Hz (for SFO and MnPO) delivered via a custom-made optic cable using a pulse generator (World Precision Instruments). The laser intensity was maintained at 5 mW (for OVLT) or 10 mW (for SFO and MnPO) at the tip of the fibre.

Behavioural assays.

For water-restriction experiments, mice were provided with 1 ml of water daily. For food-restriction experiments, mice were provided with 0.5 pellets per 20 grams of body weight daily. All assays were performed in a modified lickometer as described previously[39] or a Biodaq monitoring system (Research Diets Inc.). For all photometry assays, mice were acclimatized for 10–15 min in the lickometer cage before stimuli were given.

Long-term access assays.

For optogenetic testing (Fig. 1g and Extended Data Fig. 2c, e), satiated mice were given *ad libitum* access to water with photostimulation. Photostimulation was delivered for 1 s at 3-s intervals throughout the behavioural sessions. For Fig. 2e and Extended Data Fig. 6c, mice were given access to water for 20 min after 24-h water restriction, and photostimulation was delivered for the first 10 min. For feeding assays (Fig. 2e), mice were single-housed in Biodaq cages after 24-h food restriction, and chow intake was measured for 20 min with or without light stimulation. For acute inhibition experiments, mice were given access to 150 mM NaCl (Fig. 5b and Extended Data Fig. 8c) or water (Fig. 1g and 2e, Extended Data Figs 8a, b, d) for 20–30 min after 24 h water restriction, or 300 mM sucrose (Fig. 1g and Extended Data Fig. 2e) after food restriction. For all acute inhibition experiments, CNO was injected at 10 mg kg^{-1} body weight, 30 min before the start of the behaviour session. For acute activation experiments, CNO was injected at 1 mg kg^{-1} body weight (Extended Data Fig. 7e), 30 min before the start of the behaviour session. For Fig. 3a and Extended Data Figs 4a and 8f, access to water or saline was provided for 30 min after 24 h of water restriction. For Fig. 4a, water or HydroGel (ClearH$_2$O) in a cup was provided for 30 min after 24 and 36 h of water restriction, respectively. The weight of the cup was measured before and after the behaviour session. For Fig. 4d, 0.5 pellets of chow was provided for 30 min after 24 h of food restriction. The entire session was recorded using a camera at 30 frames per second, and ingestion episodes were manually annotated.

Salt- or mannitol-loading experiments.

150 μl or 300 μl of 2 M NaCl, or 300 μL of 2 M mannitol, was injected intraperitoneally at the end of the acclimatization period. For Fig. 1i and Extended Data Fig. 2f, CNO or vehicle (water) was injected 10 min before the injection of NaCl or mannitol.

Brief access assays.

For optogenetic experiments, behavioural assays were performed essentially as previously described[19]. Satiated mice were tested in a gustometer for 10–15 trials (Fig. 1e and Extended Data Fig. 1d). The laser pulses were delivered for 20 s of the 40-s trial. After the first lick, mice were given access to a water spout for 5 s. For photometry recording (Fig. 3b and Extended Data Fig. 7a), water-restricted mice were presented with one of the following four stimuli for 30 s: water, isotonic saline, silicone oil or empty bottle (control). Under food-restricted conditions (Fig. 3c and Extended Data Fig. 7b), a bottle containing 300 mM sucrose, peanut butter coated on a spout, or an empty bottle was presented for 30 s. To avoid the effect of internal state changes, we used the data from the first stimulus presentation in each session. To test the effect of temperature (Fig. 4f), three bottles of water at 4 °C, room temperature (25 °C) or 37 °C were placed at the start of the acclimatization period (10 min). Each trial was 30 s long with an inter-trial interval of 2 min. For Fig. 4e, water-restricted mice had access to water for 2 s repeated 15 times or for one 30-s period. Each presentation was followed by a 30-s interval.

Fibre photometry.

We measured bulk fluorescence signals using fibre photometry as previously described[31]. In brief, 490 nm and 405 nm light-emitting diodes (Thorlabs, M490F1 and M405F1) were collimated and delivered to the brain. The light intensity was maintained at less than 100 μW during all recordings. The fluorescence signal was then focused onto a femtowatt photoreceiver (Newport, Model 2151). The modulation and demodulation were performed with an RP2.1 real time processor (Tucker-Davis Technologies) running custom software. The licks from the lickometer were simultaneously recorded as real-time transistor-transistor logic signals to the RP2.1. Fluorescence changes were analysed using custom MATLAB (MathWorks) code as described previously[31]. Data were extracted and subjected to a low-pass filter at 1.8 Hz. A linear function was used to scale up the 405-nm channel signal to the 490-nm channel signal to obtain the fitted 405-nm signal. The resultant $\Delta F/F$ was calculated as (raw 490 nm signal – fitted 405 nm signal)/(fitted 405 nm signal). For brief access tests, the area under the curve ($\Sigma \Delta F_{during}$) was quantified by integrating the fluorescence signals during the bout. For all bouts, the mean fluorescence for 30 s before the first lick was calculated and subtracted from the entire session. ΔF changes ($\Delta F_{post} - \Delta F_{pre}$) were calculated by subtracting the mean fluorescence signal during the 2-s period before the first lick from the mean signal during the 2-s period at 1 min after the bout. To display traces, the fluorescence data was time-binned by a factor of $2.5 \times$ the sampling frequency and down-sampled to 1 Hz. For long-term tests, the area under the curve was calculated for 2.5 min after the start of the bout. Changes in ΔF were calculated by subtracting the mean signal during the 2-s period before the first lick or NaCl injection from the mean signal during the 2-s period at 5 or 10 min after the bout (Extended Data Fig. 4). For peristimulus time histograms (Fig. 4c, d), the first bout at the start of the session and the last bout within 10 min of access were used. The areas under the curve for the peristimulus time histograms were calculated during the first or the last 15 s.

Viral tracing.

Monosynaptic rabies tracing. 150 nl of a mixture of AAV1-CA-FLEX-RG and AAV1-EF1a-FLEX-TVA-mCherry (4:1 ratio) was injected to the target area. Two weeks later, 200 nl of EnvA G-deleted Rabies-eGFP was injected into the same area. The mice were euthanized a week later and their brains collected.

HSV tracing.

200 nl of a mixture of AAV1-Syn-GCaMP6s-WPRE-SV40 and hEF1-LS1L-mCherry HT (2:5 ratio) was injected to the SFO of *Vgat-cre* mice. The GCaMP virus was used to mark the injection site. The mice were euthanized three weeks later and their brains collected.

The sections were imaged using a confocal microscope (TCS SP8, Leica) or a slide scanner (VS120, BX61VS, Olympus) at $20 \times$. The slide scanner images were used to count cells using ImageJ. Representative images in Figs 1a, 2a and Extended Data Fig. 5 are from the confocal microscope. Regions with an average greater than 10 rabies-virus-positive cells were included in the analysis.

Histology.

Mice were deeply anaesthetized with carbon dioxide and then transcardially perfused with PBS followed by 4% paraformaldehyde in PBS (pH 7.4) at 4 °C. The brains were extracted and fixed in 4% paraformaldehyde at 4 °C overnight. 100 μm coronal sections were prepared using a vibratome (Leica, VT-1000 s) for antibody staining. The primary antibodies (1:500 dilution) used were: goat anti-c-Fos (Santa Cruz, SC-52G), rabbit anti-NOS1 (Santa Cruz, sc-648), rabbit anti-GAD65$^+$GAD67 (Abcam, ab183999), chicken anti-GFP (Abcam, ab13970) and rat anti-mCherry (Thermo Fisher, M11217). After washing three times with PBS, the sections were incubated with secondary antibodies (1:500 dilution) in blocking buffer for 4 h. The GAD65/67 primary/secondary antibody incubation solution was prepared without detergent. Fluorescence *in situ* hybridization was carried out using the RNAscope fluorescent multiplex kit (Advanced Cell Diagnostics) in accordance with the manufacturer's instructions. *Glp1r-cre*/Ai9 mice were used with probes targeted to tdTomato and GLP1R.

RNA sequencing analysis.

The dorsal lamina terminalis in *Vgat-cre*/Ai9 mice were dissected under a fluorescence microscope. To minimize contamination from other tissues, the lamina terminalis tissue containing the SFO and dorsal MnPO were peeled off. For non-lamina-terminalis control, we dissected small tissues of the cortex from the same mice. These samples were dissociated into single cells using the Papain Dissociation System (Worthington), labelled with 4′,6-diamidino-2-phenylindole (DAPI) and the tdTomato-positive neurons were sorted using a flow cytometer (MoFlo Astrios, Beckman Coulter). RNA was extracted using a PicoPure RNA isolation kit (Applied Biosystems) and complementary DNA was prepared using an Ovation RNA-seq V2 kit (Nugen). Relative gene expression (Fig. 2b) was calculated as a ratio of fragments per kilobase million of the dorsal lamina terminalis to that of the cortex. The genes with fragments per kilobase million < 0.1 in the cortex were omitted from the plot.

Slice electrophysiology.

Procedures for the preparation of acute brain slices and recordings with optogenetic stimulations were similar to those described previously[19,43]. After decapitation, the brain was removed and immersed in ice-cold solution. Coronal slices (300 mm) were cut using a vibratome (VT-1200 s, Leica) and moved into HEPES holding solution (in mM: NaCl 92, KCl 2.5, NaH$_2$PO$_4$ 1.2, NaHCO$_3$ 30, HEPES 20, glucose 25, Na-ascorbate 5, thiourea 2, Na-pyruvate 3, MgSO$_4$ 2, CaCl$_2$ 2, at pH 7.35). The slices were allowed to recover at 33 °C for 30 min and then held at room temperature (around 25 °C) until use.

While recording, slices were perfused continuously (around 2 ml min^{-1}) with artificial cerebrospinal fluid (in mM: NaCl 124, KCl 2.5, NaH$_2$PO$_4$ 1.2, NaHCO$_3$ 24, glucose 25, MgSO$_4$ 1, CaCl$_2$ 2) at 25 °C. Neurons were visualized and targeted using an upright infrared differential interference contrast microscope (BX51WI, Olympus). Whole-cell recordings were achieved using glass pipettes with an impedance of 4–6 MΩ when filled with intracellular solution (for voltage clamp, in mM: CsCl 145, NaCl 2, HEPES 10, EGTA 0.2, QX-314 Chloride 5, Mg-ATP 4, Na-GTP 0.3, at pH 7.25; for current clamp, in mM: K-

gluconate 145, NaCl 2, KCl 4, HEPES 10, EGTA 0.2, Mg-ATP 4, Na-GTP 0.3, at pH 7.25). Electrical signals were sampled at 20 kHz and filtered at 2.9 kHz using an EPC 10 system (HEKA Elektronik). To evaluate postsynaptic currents evoked by light pulses, the membrane potential of SFO^{nNOS} (transduced with CamKII-mCherry/eYFP) or SFO$^{non-nNOS}$ neurons was held at −60 mV. Light pulses were generated by a mercury lamp, filtered by an optical filter (Chroma) and controlled by an electronic shutter driver (VCM-D1, UNIBLITZ). 2-ms light pulses were delivered at 1 Hz four times, followed by a 4-s interval. We repeated this stimulus cycle 20 times. To confirm that the postsynaptic currents recorded were GABAergic, picrotoxin (150 μM) was applied through the bath for part of the experiments. To confirm glutamatergic postsynaptic currents, 6-cyano-7-nitroquinoxaline-2,3-dione (CNQX, 10 μM) and 2-amino-5-phosphonovaleric acid (DL-APV, 25 μM) were applied through the bath. Monosynaptic connection was defined by synaptic inhibitory or excitatory postsynaptic currents with latencies less than 16.4 ms. For hM4Di experiments, current-clamp recordings were performed by applying a constant supra-threshold current injection to produce tonic action potentials. CNO (around 6 μM) was applied using a puff (30 s) from another glass pipette placed approximately 50 μm from the recorded cell.

Plasma Na⁺ and osmolality measurements.

After the injection of 150 μl of 2 M NaCl or 300 μl of 2 M mannitol, trunk blood was collected from wild-type mice. Plasma was then extracted after centrifugation at 1500*g* for 20 min. Plasma osmolality was measured using a vapour pressure osmometer (Vapro 5520). Plasma Na$^+$ concentration was measured using Dionex (Thermo) ICS 2000.

Intra-cranial drug delivery.

100 ng of exendin-4 (Sigma Aldrich) dissolved in 1 μl of artificial cerebrospinal fluid was delivered using a custom-made cannula and tubing (PlasticsOne) connected to a Hamilton syringe driven by a pump (NewEra PumpSystems) at 100 nl min^{-1} into the MnPO of water-deprived mice under head-fixed conditions. Two minutes after infusion, freely moving mice were given access to water for the next 45 min. The cannula position was verified by infusing exendin-4-FAM (Anaspec) conjugate before euthanasia.

Enzyme-linked immunosorbent assay.

Total plasma GLP1 was measured using EZGLP1T-36k kit (Millipore) as described previously[44]. In brief, after blood was collected in EDTA-coated tubes, plasma was isolated by centrifugation at 1500*g* for 20 min. Samples were then kept at −80 °C until measurement. For food-repleted (FD + F) and water-repleted (WD + W) conditions, mice were given access to Ensure for 30 min or water for 5 min, respectively.

Statistics.

All statistical analyses were carried out using Prism (GraphPad). We used a two-tailed Mann-Whitney *U* test, a paired *t*-test or a Kruskal-Wallis one-way ANOVA, depending on the experimental paradigm. *$P < 0.05$, **$P < 0.01$, ***$P < 0.001$. Details of the tests used are outlined in Supplementary Table 1. No statistics to determine sample size, blinding or

randomization methods were used. Viral expression and implant placement was verified by histology before mice were included in the analysis. These criteria were pre-established.
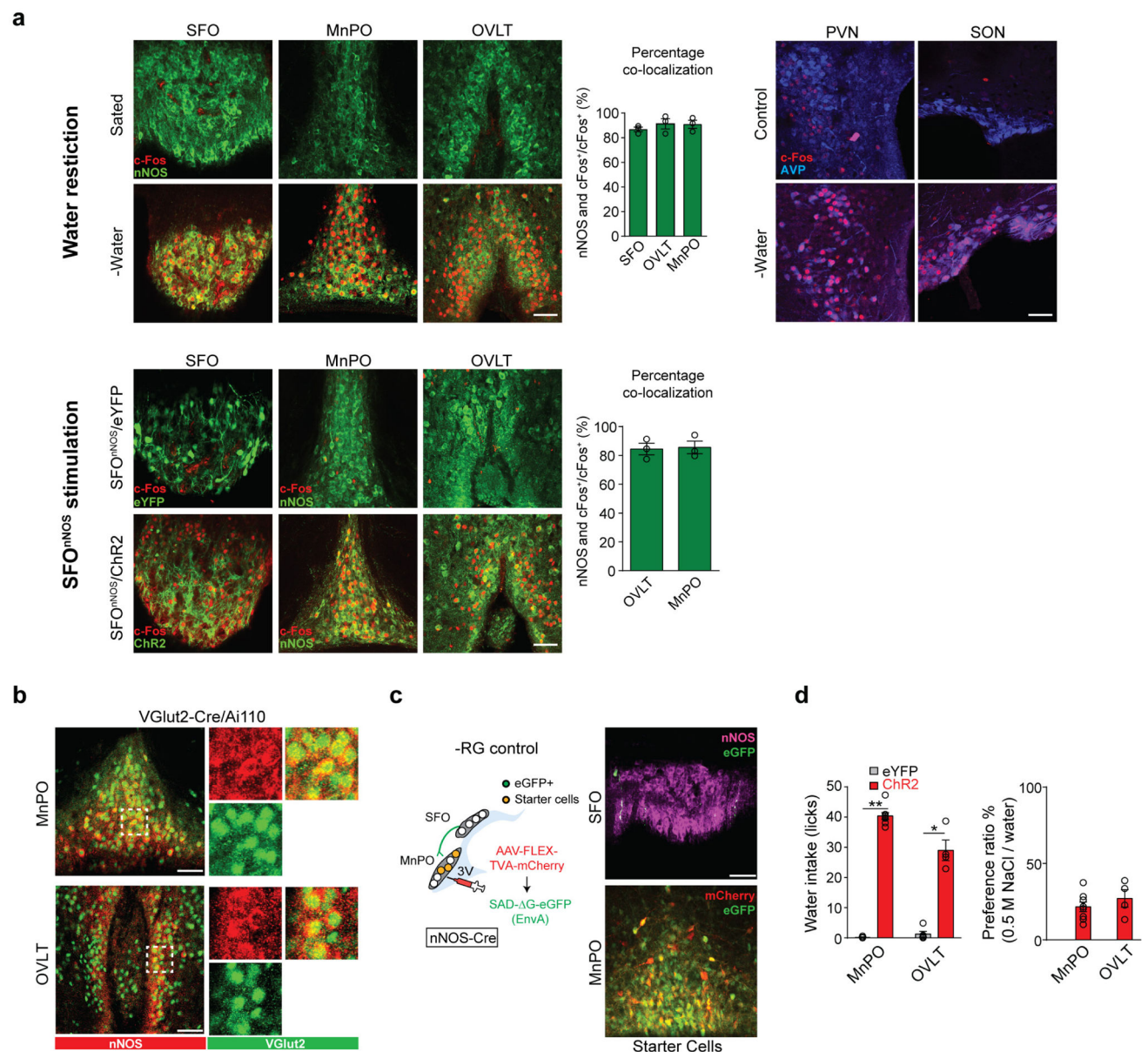
Code availability.

Custom MATLAB code used in this study is available from the corresponding author upon reasonable request.

Data availability.

Data are available from the corresponding author upon reasonable request.

Extended Data

Extended Data Figure 1 |. Optogenetic activation MnPO^{nNOS} and OVLT^{nNOS} neurons induces robust water intake in satiated mice.

a, Water restriction (top) and SFO^{nNOS} photostimulation (bottom) induces robust c-Fos expression in the SFO, MnPO and OVLT, compared to control conditions. A majority of c-Fos signals in these areas overlapped with nNOS-expressing neurons. The graph shows the quantification of the overlap between nNOS and c-Fos signals ($n = 3$ mice). c-Fos signals in the paraventricular nucleus (PVN) and supraoptic nucleus (SON) overlapped with vasopressin (AVP)-expressing neurons. **b**, MnPO (top) and OVLT (bottom) excitatory neurons visualized in VGlut2/Ai110 transgenic mice co-stained with nNOS (red, antibody staining). MnPO^{nNOS} and OVLT^{nNOS} neurons co-express a glutamatergic marker. 92.2 $\pm$ 4.9% of nNOS-expressing neurons were excitatory, and 80.9 $\pm$ 2.6% of excitatory neurons are nNOS-expressing in the MnPO ($n = 3$ mice). Magnified images are shown on the right. **c**, Left, scheme of the control experiments for monosynaptic rabies tracing. Right, a representative image of the MnPO of an *nNOS-cre* mouse transduced with AAV-EF1a-FLEX-TVA-mCherry (red) followed by EnvA G-deleted Rabies-eGFP (bottom). No eGFP$^+$ cells were present in the SFO (top, one of two mice) **d**, Photostimulation of ChR2-expressing MnPO^{nNOS} and OVLT^{nNOS} neurons (red bars, $n = 8$ and 4 mice for MnPO and OVLT respectively) triggered intense drinking; control mice infected with AAV-DIO-eYFP showed no such response (grey bars, $n = 5$ mice). Photostimulated mice showed a strong preference for water over a highly concentrated NaCl solution (500 mM, right panel). $*P < 0.05$, $**P < 0.01$; by two-tailed Mann–Whitney U test. All error bars show mean $\pm$ s.e.m. Scale bars, 50 μm.
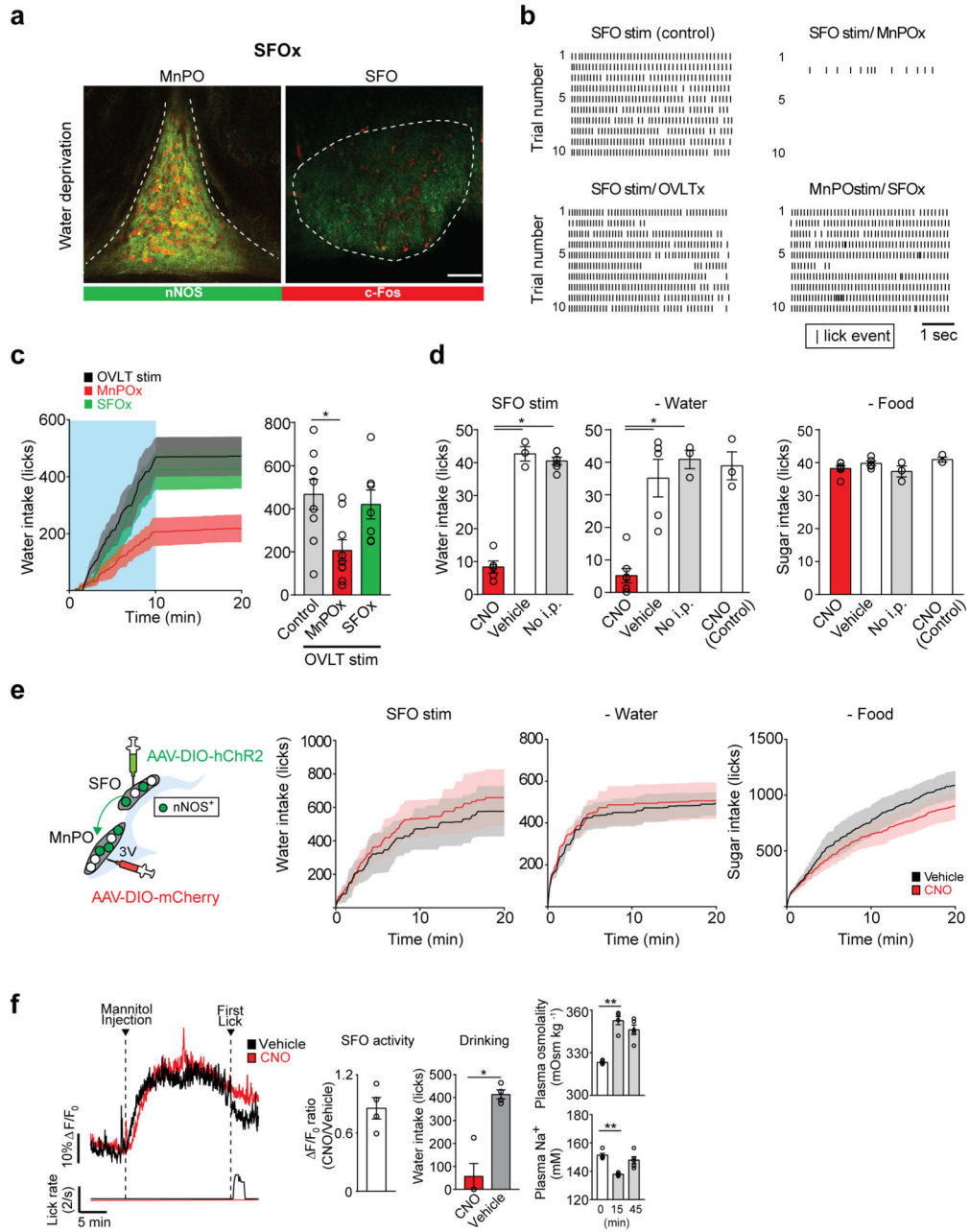
Extended Data Figure 2 |. MnPO^{nNOS} neurons are necessary for the induction of drinking by SFO^{nNOS} photostimulation.

a, Casp3-TEVp efficiently eliminates SFO^{nNOS} neurons (right) without affecting MnPO^{nNOS} neurons (left). c-Fos expression pattern is shown after water-restriction (red). **b**, Rastor plots representing licking events during the 5-s session with photostimulation. **c**, Ablation of MnPO^{nNOS} (MnPOx) but not SFO^{nNOS} (SFOx) neurons attenuated the drinking response to OVLT^{nNos} photostimulation (left, 10 min, blue box). Quantification of the number of licks during the 10-min light-on period (right, $n = 9$ mice for controls and MnPOx and $n = 7$ mice for SFOx). **d**, 5-s brief-access assays to examine the necessity of MnPO^{nNOS} neurons. Acute inhibition of MnPO^{nNOS} neurons by CNO injection severely reduced

SFO[nNOS]-stimulated (left, $n = 5$ mice for CNO, $n = 3$ mice for vehicle, and $n = 6$ mice for no i.p.) and dehydration-induced water intake (middle, $n = 7$ mice for CNO, $n = 5$ mice for vehicle, and $n = 3$ mice for no i.p.). However, the same treatment did not suppress sucrose consumption (300 mM, right, $n = 6$ mice for CNO, $n = 5$ mice for vehicle, and $n = 3$ mice for no i.p.). Control mice transduced by AAV-DIO-mCherry in the MnPO showed no reduction after water or food-restriction ($n = 3$ mice). **e**, mCherry control for Fig. 1g. Cumulative water intake in *nNOS-cre* mice transduced with AAV-DIO-mCherry in the MnPO, AAV-DIO-ChR2-eYFP in the SFO under photostimulated (left, $n = 5$ mice) or water-restricted conditions (middle, $n = 6$ mice), and sucrose (300 mM) intake under food-restricted conditions (right, $n = 5$ mice). **f**, Intraperitoneal injection of mannitol robustly activated SFO[nNOS] neurons with (red trace) or without (black trace) CNO injection (left). CNO injection drastically suppressed drinking behaviour without changing the activity of SFO[nNOS] neurons (middle, $n = 4$ mice). Plasma osmolality was increased by the injection of mannitol (right, $n = 5$ mice). *$P < 0.05$, **$P < 0.01$, by paired two-tailed t-test or Kruskal–Wallis one-way ANOVA test with Dunn's correction for multiple comparisons. All error bars and shaded areas show mean ± s.e.m. Scale bar, 50 μm.
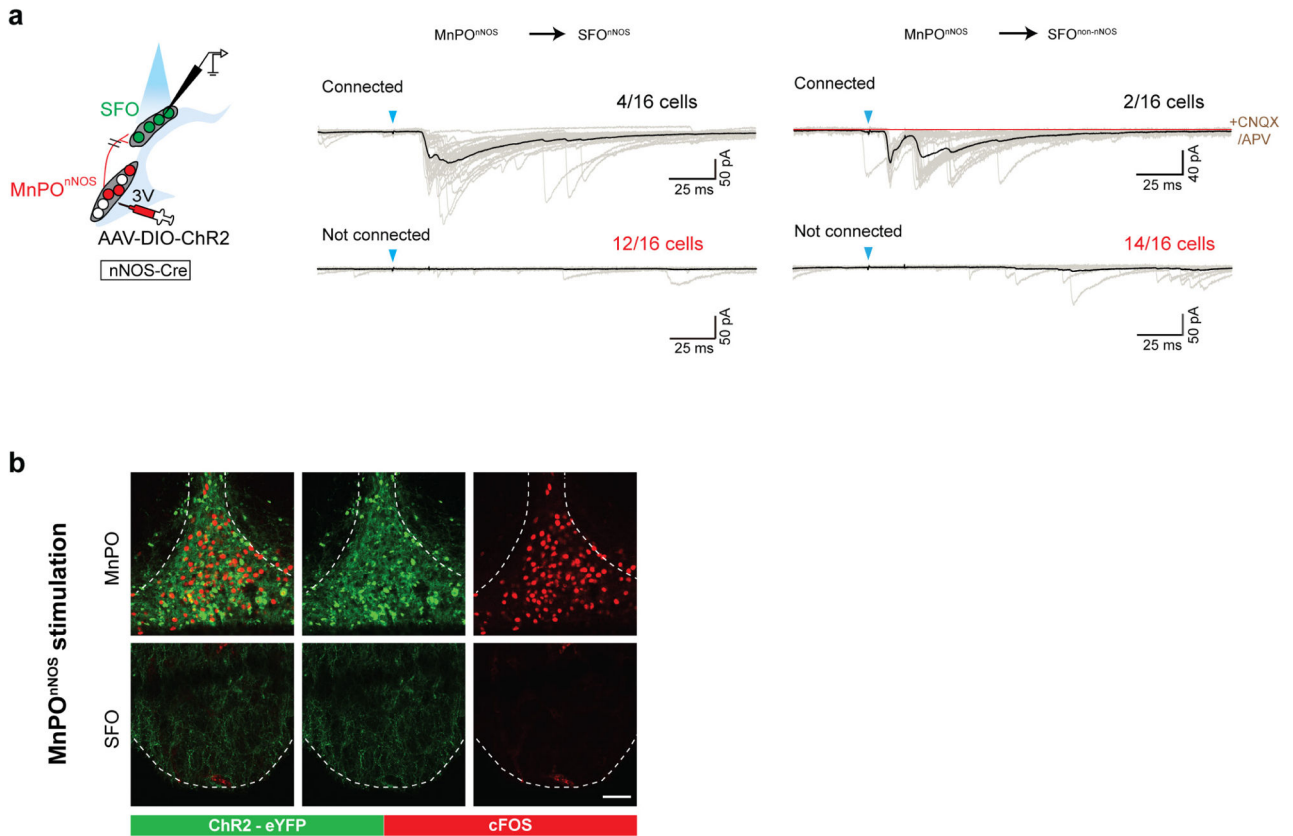
**Extended Data Figure 3 |. The SFO receives sparse monosynaptic input from MnPO[nNOS] neurons.**

a, Left, schematic for the assessment of the MnPO[nNOS] → SFO monosynaptic connection (left). Right, whole-cell patch-clamp recording from SFO neurons was performed with optogenetic stimulation of MnPO[nNOS] → SFO projections. Excitatory synaptic currents

were measured in the presence (red trace) or absence (black trace) of CNQX (10 μM) + DL-APV (25 μM) after photostimulation (2 ms, blue arrowheads). Most SFO[nNOS] neurons (12 out of 16 cells, labelled with mCherry, middle panel) or SFO[non-nNOS] neurons (14 out of 16 cells, right panel) did not receive monosynaptic input from MnPO[nNOS] neurons. **b**, Representative image (one out of three mice) of robust c-Fos expression (red) in the MnPO (top) but not in the SFO (bottom) by photostimulation of ChR2 expressing MnPO[nNOS] neurons. Scale bar, 50 μm.
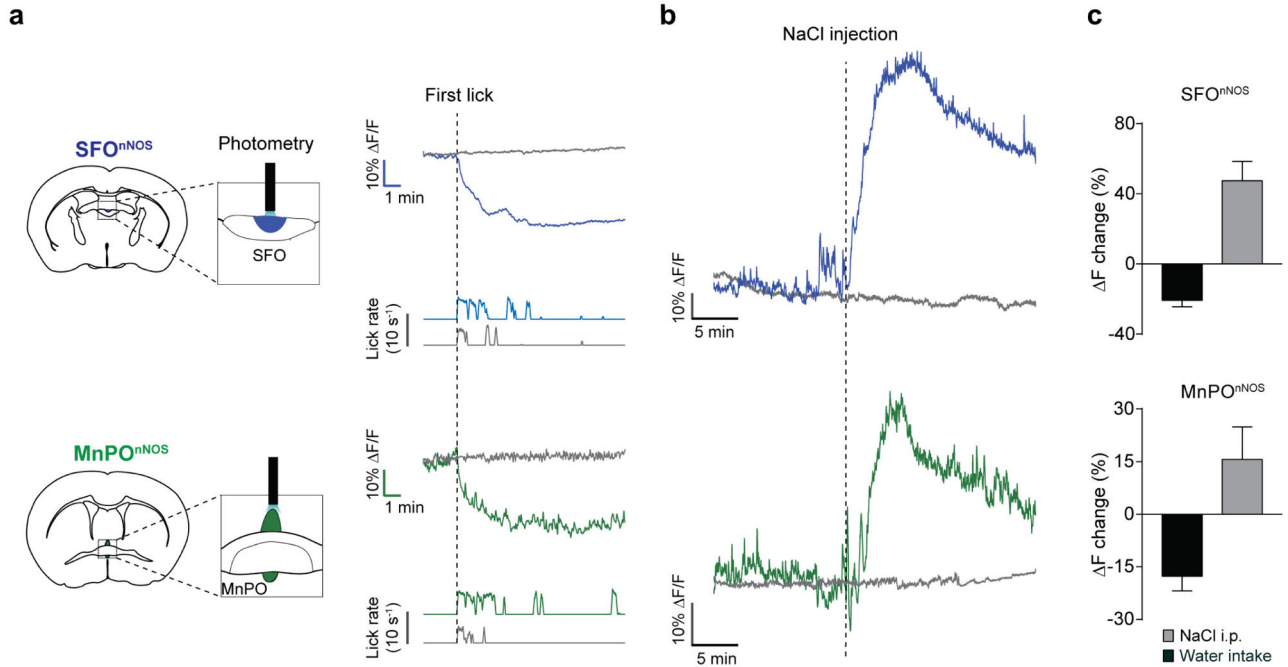
Extended Data Figure 4 |. Neural dynamics of SFO[nNOS] and MnPO[nNOS] neurons.
a, Left, Schematic of fibre photometry experiments from SFO[nNOS] (top) and MnPO[nNOS] (bottom) neurons. *nNOS-cre* mice were injected with AAV-FLEX-GCaMP6s or eYFP into the SFO and MnPO. Right, representative traces showing the real-time activity of the SFO[nNOS] (blue trace) and MnPO[nNOS] (green trace) populations with water intake in water-restricted mice. Grey traces show the activity of eYFP control mice. Corresponding lick patterns are also shown (lower traces). SFO[nNOS] and MnPO[nNOS] neurons are rapidly and persistently inhibited by water drinking. **b**, SFO[nNOS] and MnPO[nNOS] neurons are sensitive to thirst-inducing stimuli. Intraperitoneal injection of NaCl (2 M, 300 μl) in a water-satiated animal robustly activated SFO[nNOS] (blue) and MnPO[nNOS] (green) neurons. **c**, Quantification of the neuronal responses. During liquid intake (black bars, $n = 4$ mice for SFO, $n = 6$ mice for MnPO) and sodium loading (grey bars, $n = 5$ mice), both SFO[nNOS] and MnPO[nNOS] neurons showed opposite activity changes. All error bars show mean ± s.e.m.
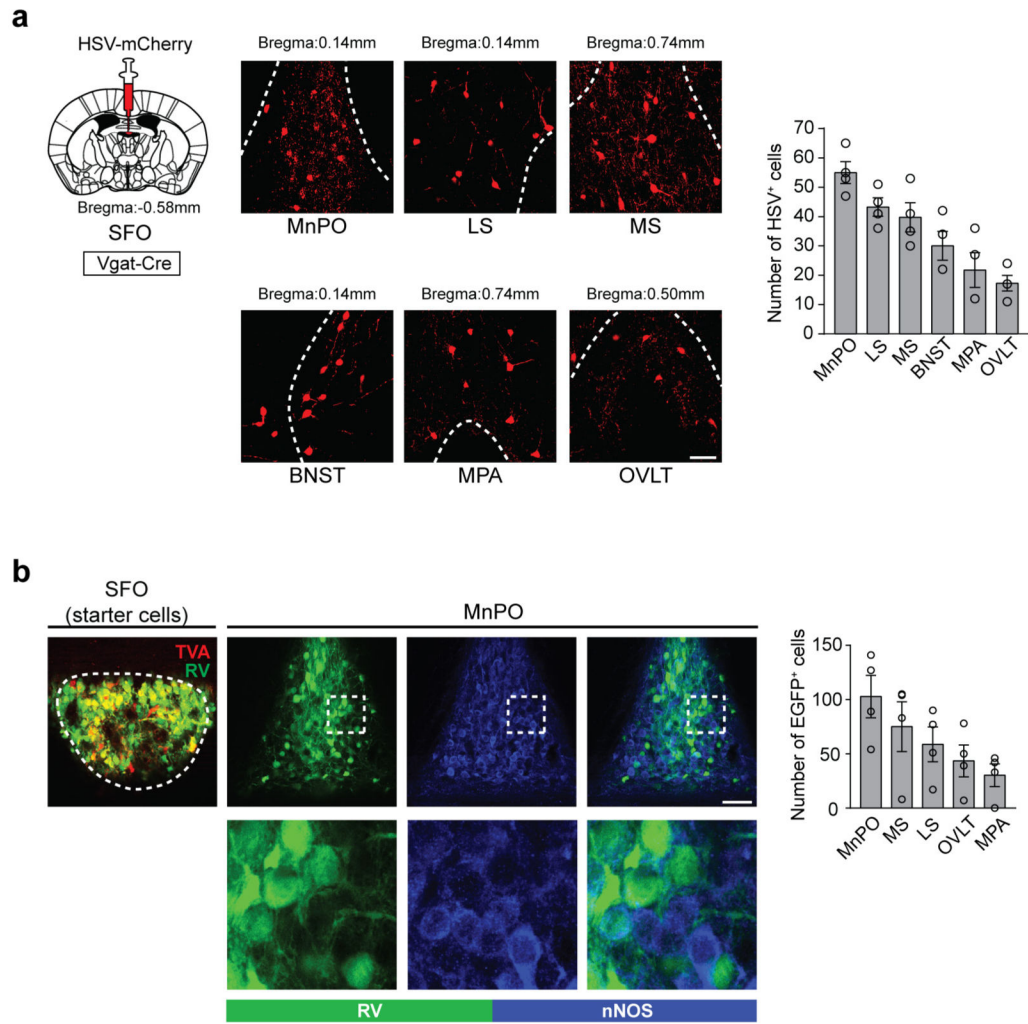
**Extended Data Figure 5 |. Mapping of inhibitory inputs to the SFO.**

a, Left, a schematic for retrograde tracing of inhibitory inputs to the SFO by HSV-mCherry. Shown are the major inhibitory inputs to the SFO. Right, quantification of HSV-positive neurons ($n = 4$ mice). LS, lateral septum; MS, medial septum; BNST, bed nucleus of the stria terminalis; MPA, medial preoptic area. **b,** Monosynaptic retrograde rabies tracing of SFO^nNOS neurons. Left, a representative image of the SFO of an *nNOS-cre* mouse transduced with AAV-CA-FLEX-RG and AAV-EF1a-FLEX-TVA-mCherry followed by EnvA G-deleted Rabies-eGFP. Right, almost no eGFP-positive neurons in the MnPO (green, $5.4 \pm 1.3\%$, $n = 4$ mice) overlapped with excitatory nNOS-expressing neurons (blue). Maximum inputs to the SFO^nNOS neurons are from the MnPO, followed by the MS, LS, MPA and OVLT ($n = 4$ mice). All error bars show mean $\pm$ s.e.m. Scale bars, 50 μm. The mouse brain in this figure has been reproduced from the mouse brain atlas[45].
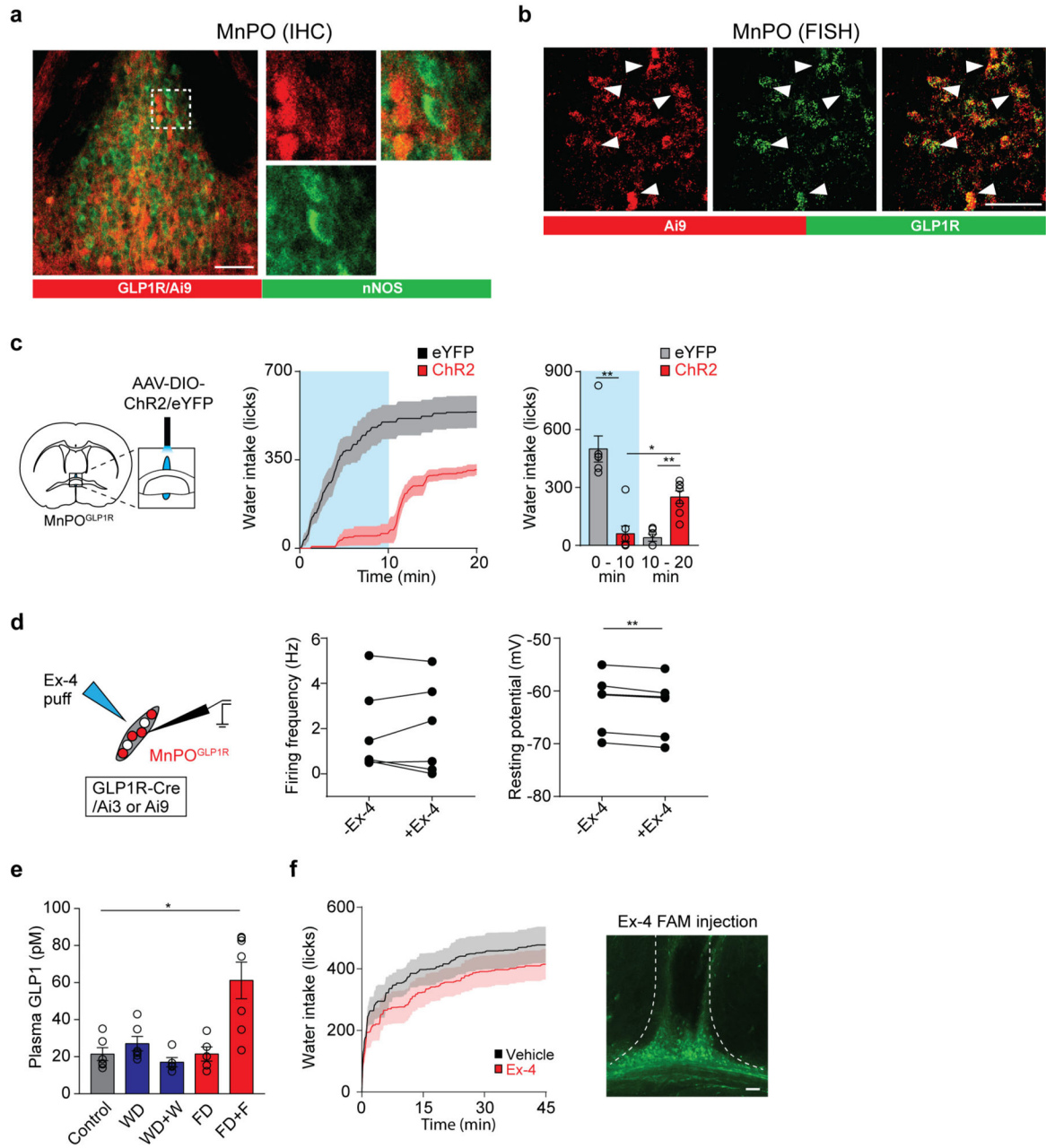
Extended Data Figure 6 |. The MnPO^GLP1R population does not overlap with nNOS-expressing neurons.

a, nNOS antibody staining (green) of the MnPO from a *Glp1r-cre/*Ai9 transgenic mouse expressing tdTomato in MnPO^GLP1R neurons (red). No substantial overlap was observed between these populations (4.3 ± 0.9% of GLP1R-expressing neurons, *n* = 3 mice). **b**, Fluorescence *in situ* hybridization (FISH) shows that a majority of Ai9 expression (red, 91.9 ± 2.4%, *n* = 3 mice) closely overlaps with endogenous GLP1R expression (green). **c**, Left, a diagram showing optogenetic stimulation of MnPO^GLP1R neurons transduced with AAV-DIO-ChR2-eYFP or AAV-DIO-eYFP. Right, stimulation of ChR2-expressing MnPO^GLP1R neurons inhibited drinking after water restriction as compared to eYFP controls (*n* = 7 mice

for ChR2, $n = 6$ mice for controls, blue box indicates the Light-ON period). For statistical analysis, we used the same dataset as for 0–10 min from Fig. 2e. **d**, GLP1 has minor effects on acute drinking behaviour. A diagram of whole-cell recording from MnPO^{GLP1R} neurons is shown on the left. A GLP1 agonist, exendin-4 (Ex-4), had no effect on the firing frequency of MnPO^{GLP1R} neurons in brain slice preparation (middle, $n = 6$ neurons). However, there was a small decrease in the resting membrane potential (right, $n = 6$ neurons). **e**, Enzyme-linked immunosorbent assay analysis of plasma GLP1 levels. Feeding behaviour induced robust plasma GLP1 secretion whereas water intake did not ($n = 5$ mice for WD + W and FD, $n = 6$ mice for control and WD, and $n = 7$ mice for FD + F). **f**, Left, intra-cranial injection of Ex-4 (red trace, $n = 7$ mice) into the MnPO had no effect on water intake after water deprivation as compared to vehicle injection (artificial cerebrospinal fluid, black trace, $n = 7$ mice). Right, a representative injection pattern visualized with fluorescent Ex-4 FAM. $*P < 0.05$, $**P < 0.01$, two-tailed Mann–Whitney U test or paired t-test or Kruskal–Wallis one-way ANOVA test with Dunn's correction for multiple comparisons. All error bars and shaded areas show mean ± s.e.m. Scale bars, 50 μm.
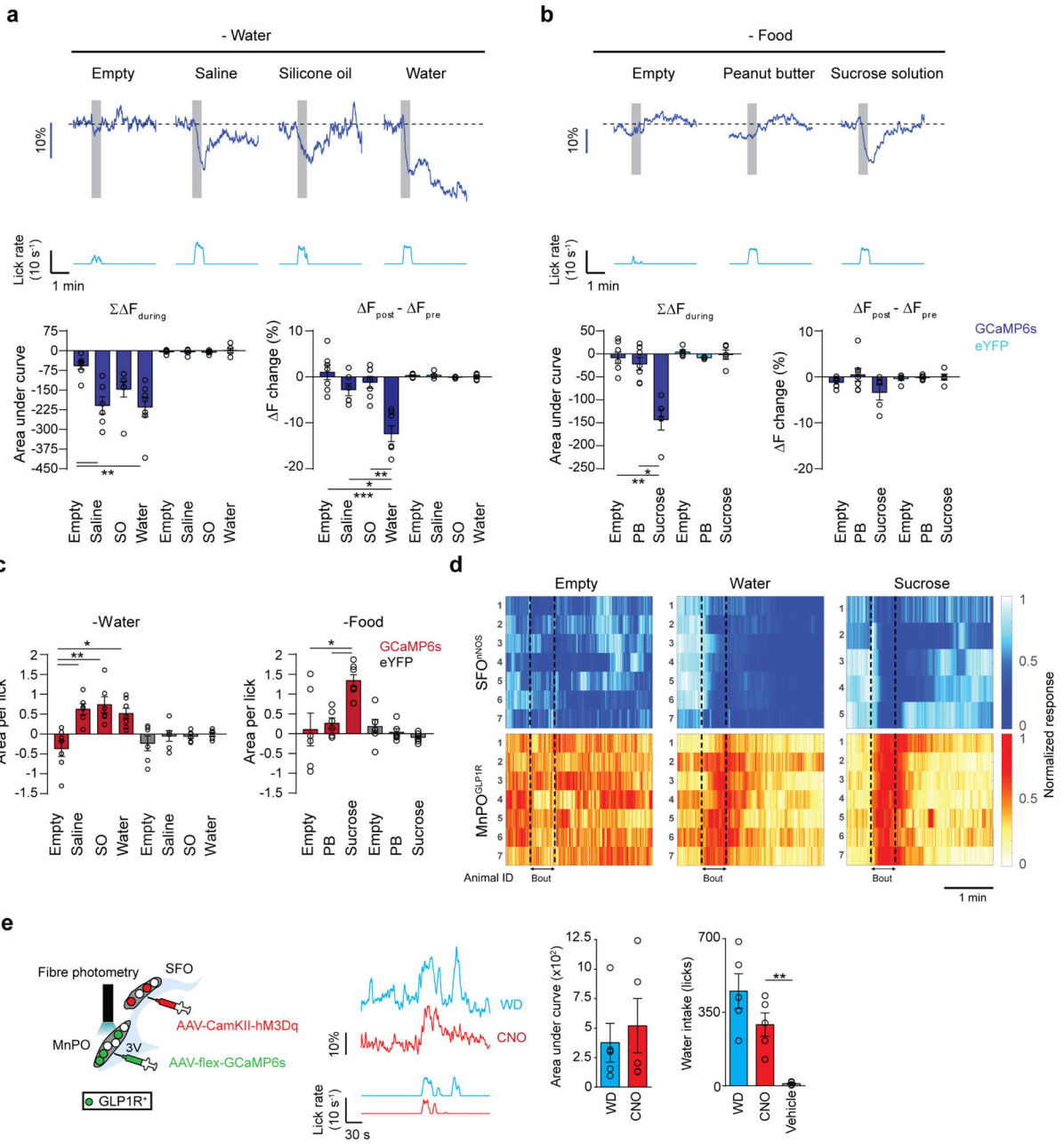
Extended Data Figure 7 |. *In vivo* activation patterns of MnPO[GLP1R] and SFO[nNOS] neurons upon ingestion.

a, SFO[nNOS] neurons are negatively and chronically regulated by water drinking. Representative responses of SFO[nNOS] (blue traces) to different types of liquids under water-restricted conditions: a control empty bottle, isotonic saline, silicone oil and water. Each stimulus was presented for 30 s (shaded box). Quantification of the responses is shown in the bottom panel. Activity change (left, area under curve) and baseline activity shift (right, ΔF change) were quantified for SFO[nNOS] neurons (GCaMP6s, dark blue bars; control, light blue bars). A significant shift in the baseline activity (ΔF change) was observed only in response to water ingestion ($n = 6$ mice for saline, $n = 7$ mice for empty, silicone oil and

water, $n = 5$ mice for eYFP). **b**, Shown are representative responses of SFO[nNOS] neurons (blue traces) to an empty bottle, peanut butter, and 300 mM sucrose solution under food-restricted conditions ($n = 7$ mice for empty and peanut butter, $n = 5$ mice for sucrose, $n = 5$ mice for all eYFP recordings). **c**, Activity change per lick was quantified for MnPO[GLP1R] neurons (GCaMP6s, red bars; eYFP, grey bars) under water-restricted conditions (left, $n = 6$ mice for saline and silicone oil, $n = 7$ mice for empty and water, $n = 6$ mice for all eYFP controls) and food-restricted conditions (right, $n = 6$ mice for empty and peanut butter, $n = 7$ mice for sucrose, $n = 6$ mice for all eYFP controls). All data were reanalysed from Fig. 3b, c. **d**, Normalized fluorescence change of SFO[nNOS] (top) and MnPO[GLP1R] (bottom) neurons from individual mice during licking an empty bottle and water under water-restricted, or sucrose under food-restricted conditions. **e**, MnPO[GLP1R] activation is independent of instinctive need. Left, fibre photometry recording of MnPO[GLP1R] neurons while activating the SFO[nNOS] neurons. GCaMP6s was virally expressed in MnPO[GLP1R] neurons for recording calcium dynamics while activating SFO[nNOS] neurons by hM3Dq-mCherry under the CamKII promoter. Middle, intraperitoneal CNO injection and water deprivation induce water drinking, which robustly activates MnPO[GLP1R] neurons (red and blue traces respectively). Right, activity change (area under the curve) and licks were quantified for natural thirst and CNO activation ($n = 5$ mice). $*P < 0.05$, $**P < 0.01$, $***P < 0.001$, paired two-tailed t-test or Kruskal–Wallis one-way ANOVA test with Dunn's correction for multiple comparisons. All error bars show mean $\pm$ s.e.m.
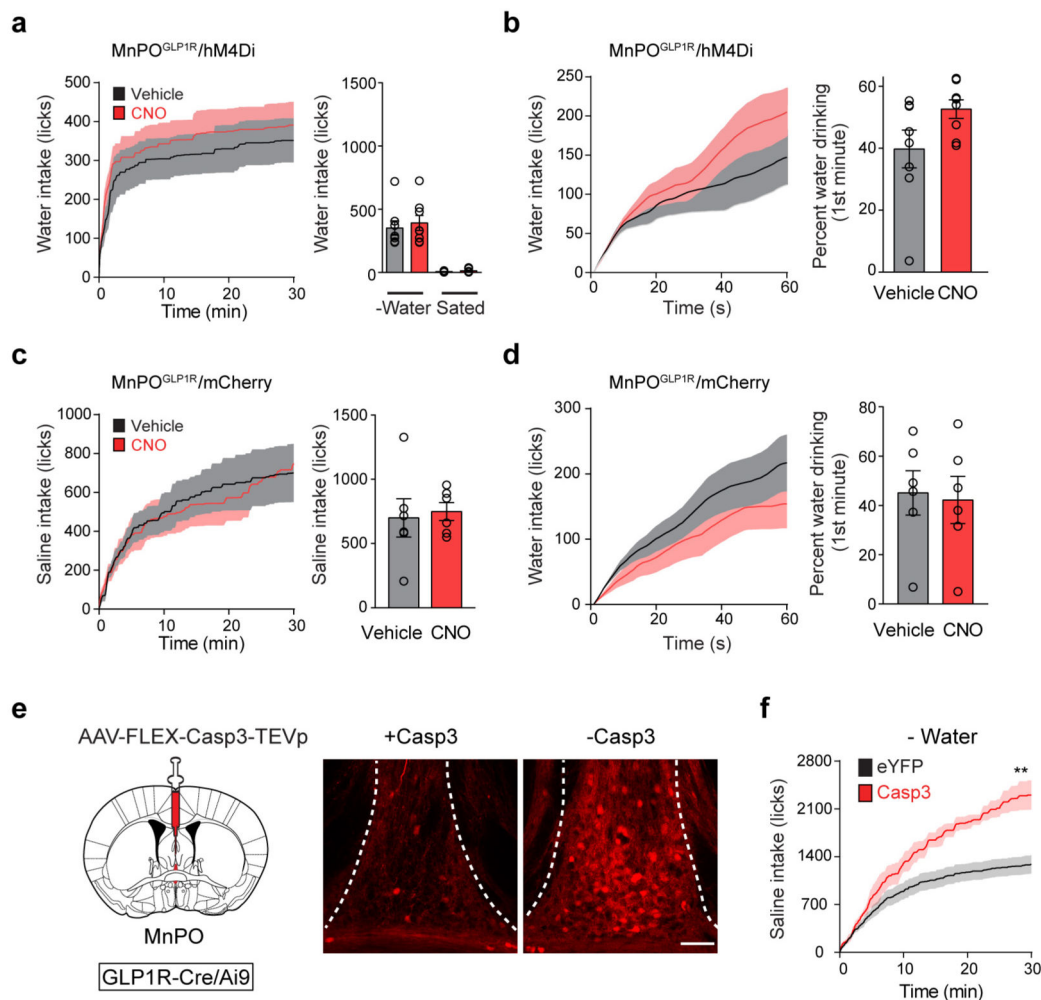
Extended Data Figure 8 |. Acute inhibition or chronic ablation of MnPO^{GLP1R} neurons causes overdrinking.

a, **b**, Acute inhibition of hM4Di-expressing MnPO^{GLP1R} neurons by CNO modestly increases water consumption at the onset of drinking. Drinking behaviour was monitored for 30 min after the injection of CNO (**a**); magnified data (0–1 min) is shown in **b** ($n = 8$ mice). **c**, **d**, mCherry controls for acute inhibition of MnPO^{GLP1R} neurons. Drinking behaviour was monitored for 30 min after the injection of CNO or vehicle under water-deprived conditions with free access to saline (**c**) or water (**d**). No significant difference was found between mice injected with CNO and vehicle ($n = 6$ mice). **e**, Schematic for the genetic ablation of MnPO^{GLP1R} neurons with AAV-flex-Casp3-TEVp (left) in *Glp1r-cre*/Ai9 mice. Compared to a control animal (right), a Casp3-injected animal displayed almost no GLP1R-expressing neurons in the MnPO (middle, representative image from one out of four mice). In both cases, GLP1R-expressing neurons were labelled using *Glp1r-cre*/Ai9 transgenic mice. **f**, Genetic ablation of MnPO^{GLP1R} neurons (red trace, $n = 4$ mice) recapitulates the overdrinking phenotype similar to the acute inhibition by hM4Di (Fig. 5b), compared to control eYFP group (black trace, $n = 6$ mice). **$P < 0.01$, by two-tailed Mann–Whitney U test. All error bars and shaded areas show mean ± s.e.m. Scale bar, 50 μm. The mouse brain in this figure has been reproduced from the mouse brain atlas[45].

a

b
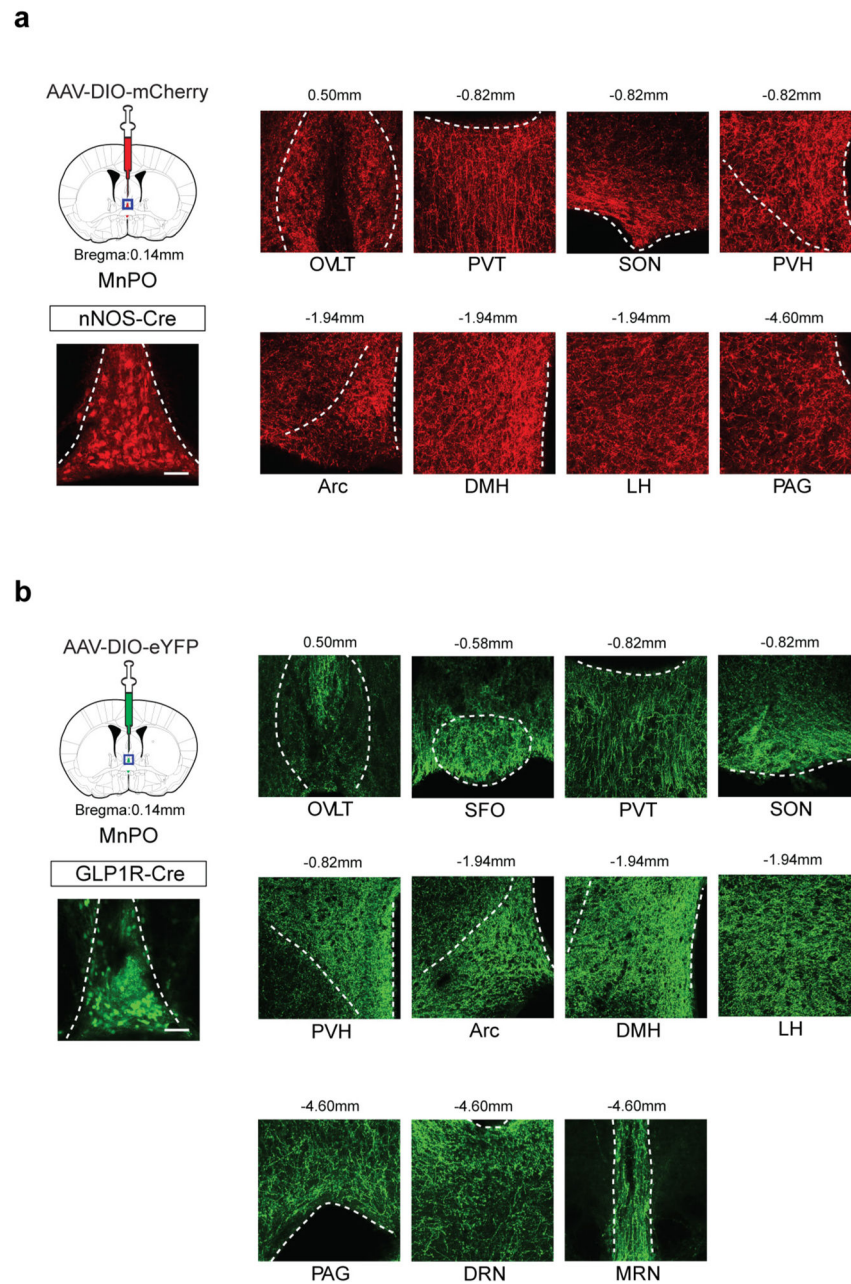
Extended Data Figure 9 |. Neural projections from nNOS[+] and GLP1R^{+} MnPO neurons.
a, **b**, Left, schematics for mapping downstream targets of MnPO neurons using AAV-DIO-mCherry (**a**) or AAV-DIO-eYFP (**b**). Right, the major outputs from MnPO neurons. *nNOS-cre* (**a**) and *Glp1r-cre* (**b**) mice were injected with AAV-DIO-mCherry and AAV-DIO-eYFP in the MnPO respectively, and the axon projections were examined using reporter expression. Shown are the injection sites and main representative downstream targets (one out of three mice). Arc, Arcuate Nucleus; DMH, dorsomedial hypothalamic nucleus; DRN, dorsal raphe nucleus; LH, lateral hypothalamus; MRN, median raphe nucleus; PAG, periaqueductal gray; PVH, paraventricular hypothalamic nucleus; PVT, paraventricular

thalamic nucleus; SON, supraoptic nucleus. Scale bars, 50 μm. The mouse brain in this figure has been reproduced from the mouse brain atlas[45].

Supplementary Material

Refer to Web version on PubMed Central for supplementary material.

Acknowledgements

References

1. Ramsay DJ & Booth D (eds) Thirst: Physiological and Psychological Aspects. Ch. 5, 6, 9-12, 19 (Springer, 1991).

2. Bourque CW Central mechanisms of osmosensation and systemic osmoregulation. Nat. Rev. Neurosci 9, 519–531 (2008).18509340

3. Fitzsimons JT Angiotensin, thirst, and sodium appetite. Physiol. Rev 78, 583–686 (1998).9674690

4. McKinley MJ & Johnson AK The physiological regulation of thirst and fluid intake. News Physiol. Sci 19, 1–6 (2004).14739394

5. Johnson AK & Gross P M. Sensory circumventricular organs and brain homeostatic pathways. FASEB J 7, 678–686 (1993).8500693

6. Saker P et al. Regional brain responses associated with drinking water during thirst and after its satiation. Proc. Natl Acad. Sci. USA 111, 5379–5384 (2014).24706817

7. Seckl JR , Williams TD & Lightman SL Oral hypertonic saline causes transient fall of vasopressin in humans. Am. J. Physiol 251, R214–R217 (1986).3740301

8. Stricker EM & Hoffmann ML Presystemic signals in the control of thirst, salt appetite, and vasopressin secretion. Physiol. Behav 91, 404–412 (2007).17482653

9. Thrasher TN , Nistal-Herrera JF , Keil LC & Ramsay DJ Satiety and inhibition of vasopressin secretion after drinking in dehydrated dogs. Am. J. Physiol 240, E394–E401 (1981).7013497

10. Zimmerman CA et al. Thirst neurons anticipate the homeostatic consequences of eating and drinking. Nature 537, 680–684 (2016).27487211

11. Farrell MJ et al. Cortical activation and lamina terminalis functional connectivity during thirst and drinking in humans. Am. J. Physiol. Regul. Integr. Comp. Physiol 301, R623–R631 (2011). 21677275

12. Gizowski C , & Bourque CW The neural basis of homeostatic and anticipatory thirst. Nat. Rev. Nephrol 14, 11–25 (2018).29129925

13. Andermann ML & Lowell BB Toward a wiring diagram understanding of appetite control. Neuron 95, 757–778 (2017).28817798

14. Sternson SM Hypothalamic survival circuits: blueprints for purposive behaviors. Neuron 77, 810–824 (2013).23473313

15. Zimmerman CA , Leib DE & Knight ZA Neural circuits underlying thirst and fluid homeostasis. Nat. Rev. Neurosci 18, 459–469 (2017).28638120

16. Denton DA , McKinley MJ & Weisinger RS Hypothalamic integration of body fluid regulation. Proc. Natl Acad. Sci. USA 93, 7397–7404 (1996).8693005

17. McKinley MJ et al. in The Sensory Circumventricular Organs of the Mammalian Brain Vol. 172 (ed. McKinley MJ) (Springer, 2003).

18. Allen WE et al. Thirst-associated preoptic neurons encode an aversive motivational drive. Science 357, 1149–1155 (2017).28912243

19. Oka Y , Ye M & Zuker CS Thirst driving and suppressing signals encoded by distinct neural populations in the brain. Nature 520, 349–352 (2015).25624099

20. Simpson JB & Routtenberg A Subfornical organ: site of drinking elicitation by angiotensin II. Science 181, 1172–1175 (1973).4353653

21. Smith PM , Beninger RJ & Ferguson AV Subfornical organ stimulation elicits drinking. Brain Res. Bull 38, 209–213 (1995).7496814

22. Betley JN et al. Neurons for hunger and thirst transmit a negative-valence teaching signal. Nature 521, 180–185 (2015).25915020

23. Nation HL , Nicoleau M , Kinsman BJ , Browning KN & Stocker SD DREADD-induced activation of subfornical organ neurons stimulates thirst and salt appetite. J. Neurophysiol 115, 3123–3129 (2016).27030736

24. Abbott SB , Machado NL , Geerling JC & Saper CB Reciprocal control of drinking behavior by median preoptic neurons in mice. J. Neurosci 36, 8228–8237 (2016).27488641

25. Matsuda T et al. Distinct neural mechanisms for the control of thirst and salt appetite in the subfornical organ. Nat. Neurosci 20, 230–241 (2017).27991901

26. Miselis RR , Shapiro RE & Hand PJ Subfornical organ efferents to neural systems for control of body water. Science 205, 1022–1025 (1979).472723

27. Boyden ES , Zhang F , Bamberg E , Nagel G & Deisseroth K Millisecondtimescale, genetically targeted optical control of neural activity. Nat. Neurosci 8, 1263–1268 (2005).16116447

28. Wickersham IR et al. Monosynaptic restriction of transsynaptic tracing from single, genetically targeted neurons. Neuron 53, 639–647 (2007).17329205

29. Yang CF et al. Sexually dimorphic neurons in the ventromedial hypothalamus govern mating in both sexes and aggression in males. Cell 153, 896–909 (2013).23663785

30. Roth BL DREADDs for neuroscientists. Neuron 89, 683–694 (2016).26889809

31. Lerner TN et al. Intact-brain analyses reveal distinct information carried by SNc dopamine subcircuits. Cell 162, 635–647 (2015).26232229

32. Richards P et al. Identification and characterization of GLP-1 receptor-expressing cells using a new transgenic mouse model. Diabetes 63, 1224–1233 (2014).24296712

33. Petreanu L , Huber D , Sobczyk A & Svoboda K Channelrhodopsin-2-assisted circuit mapping of long-range callosal projections. Nat. Neurosci 10, 663–668 (2007).17435752

34. McKay NJ , Galante DL & Daniels D Endogenous glucagon-like peptide-1 reduces drinking behavior and is differentially engaged by water and food intakes in rats. J. Neurosci 34, 16417–16423 (2014).25471579

35. Betley JN , Cao ZF , Ritola KD & Sternson SM Parallel, redundant circuit organization for homeostatic control of feeding behavior. Cell 155, 1337–1350 (2013).24315102

36. Cunningham JT , Beltz T , Johnson RF & Johnson AK The effects of ibotenate lesions of the median preoptic nucleus on experimentally-induced and circadian drinking behavior in rats. Brain Res 580, 325–330 (1992).1504809

37. McKinley MJ , Mathai ML , Pennington G , Rundgren M & Vivas L Effect of individual or combined ablation of the nuclear groups of the lamina terminalis on water drinking in sheep. Am. J. Physiol. Regul. Integr. Comp. Physiol 276, R673–R683 (1999).

38. McKinley MJ et al. The median preoptic nucleus: front and centre for the regulation of body fluid, sodium, temperature, sleep and cardiovascular homeostasis. Acta Physiol. (Oxf.) 214, 8–32 (2015).25753944

39. Oka Y , Butnaru M , von Buchholtz L , Ryba NJ & Zuker CS High salt recruits aversive taste pathways. Nature 494, 472–475 (2013).23407495

40. Yarmolinsky DA , Zuker CS & Ryba NJ Common sense about taste: from mammals to insects. Cell 139, 234–244 (2009).19837029

41. Zocchi D , Wennemuth G & Oka Y The cellular mechanism for water detection in the mammalian taste system. Nat. Neurosci 20, 927–933 (2017).28553944

42. Thrasher TN , Keil LC & Ramsay DJ Drinking, oropharyngeal signals, and inhibition of vasopressin secretion in dogs. Am. J. Physiol. Regul. Integr. Comp. Physiol 253, R509–R515 (1987).

43. Krashes MJ et al. An excitatory paraventricular nucleus to AgRP neuron circuit that drives hunger. Nature 507, 238–242 (2014).24487620

44. Kahles F et al. GLP-1 secretion is increased by inflammatory stimuli in an IL-6-dependent manner, leading to hyperinsulinemia and blood glucose lowering. Diabetes 63, 3221–3229 (2014). 24947356

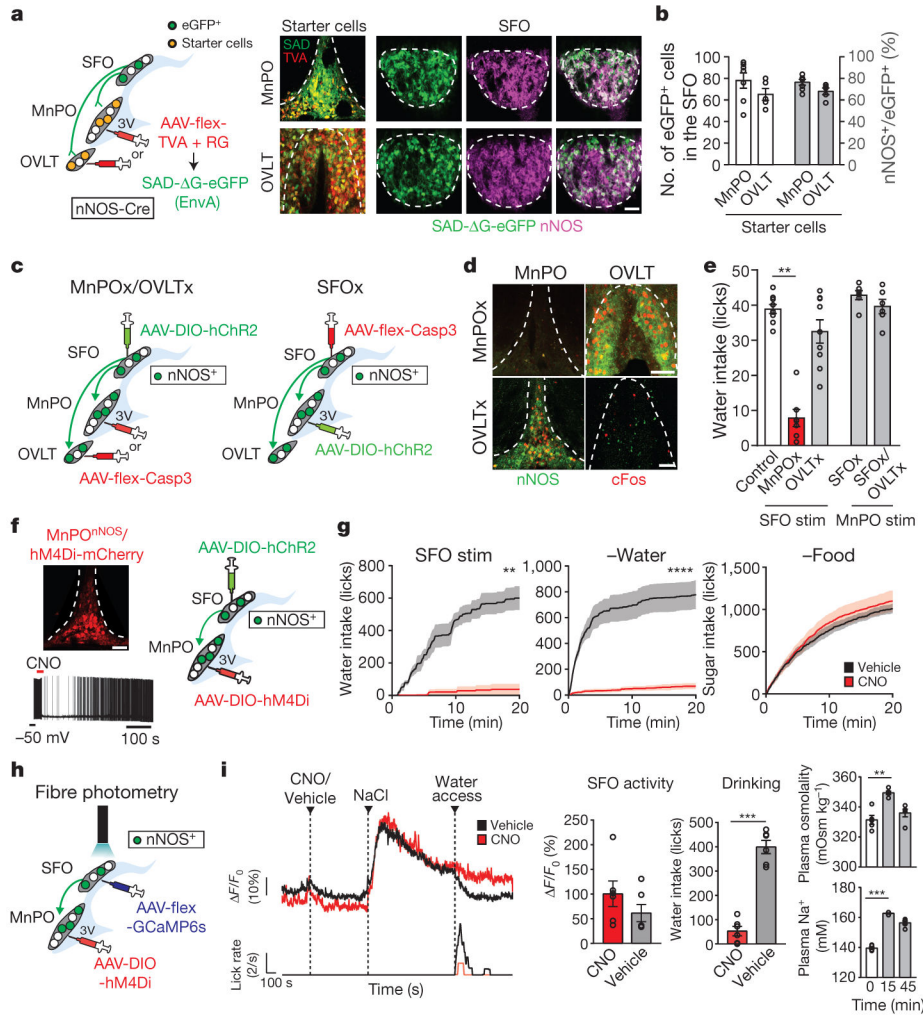45. Paxinos G & Franklin KBJ The Mouse Brain in Stereotaxic Coordinates 2nd edn (Academic, 2001).

Figure 1 |. Thirst-driving neurons are organized hierarchically in the lamina terminalis.
a, Schematic of monosynaptic rabies tracing (left). Representative images of the MnPO (top right, one of seven mice) and OVLT (bottom right, one of five mice) of an *nNOS-cre* mouse transduced with AAV-CA-flex-RG and AAV-EF1a-flex-TVA-mCherry (red) followed by RV-SAD- G-eGFP (green). 3V, third ventricle. **b**, Quantification of eGFP$^+$ neurons in the SFO ($n = 7$ and 5 mice for MnPO and OVLT, respectively). **c**, Neural epistasis analysis of the circuits of the lamina terminalis by loss-of-function manipulation. Caspase expression is induced in the MnPO, OVLT (left) or SFO (right) of *nNOS-cre* mice. **d**, Casp3-TEVp efficiently eliminates nNOS-expressing neurons (green) in the MnPO ($93.2 \pm 2.5\%$, $n = 4$ mice) and OVLT ($90.6 \pm 1.4\%$, $n = 6$ mice). c-Fos expression (red) upon the stimulation of SFO^{nNOS} neurons is shown. **e**, Number of licks during the 5-s session ($n = 9$ mice for controls and OVLTx, $n = 7$ mice for MnPOx, $n = 6$ mice for SFOx and SFOx/OVLTx). **f**, Chemogenetic inhibition of MnPO^{nNOS} neurons by CNO (left, six out of six neurons), and a diagram of photostimulation of SFO^{nNOS} and chemogenetic inhibition of MnPO^{nNOS} neurons (right). **g**, Cumulative water intake in SFO^{nNOS}-stimulated mice (left, $n = 5$ mice) or water-restricted mice (middle, $n = 10$ mice for CNO and $n = 9$ mice for vehicle), and sucrose (300 mM) intake in food-restricted mice (right, $n = 10$ mice for CNO and $n = 9$ mice for

vehicle). **h**, Fibre photometry of SFO^{nNOS} neurons while MnPO^{nNOS} neurons are inhibited by hM4Di-mCherry. **i**, Intraperitoneal NaCl injection robustly activates SFO^{nNOS} neurons with (red trace) or without (black trace) CNO injection (left and middle left). By contrast, CNO injection drastically suppressed drinking behaviour (middle right, $n = 6$ mice). Plasma osmolality (top right) and Na$^+$ concentration (bottom right) were measured after NaCl injection ($n = 5$ mice). **$P < 0.01$, ***$P < 0.001$, ****$P < 0.0001$, by Mann–Whitney U test, paired two-tailed t-test or Kruskal–Wallis one-way analysis of variance (ANOVA) test. All error bars and shaded areas show mean ± s.e.m. Scale bars, 50 μm.
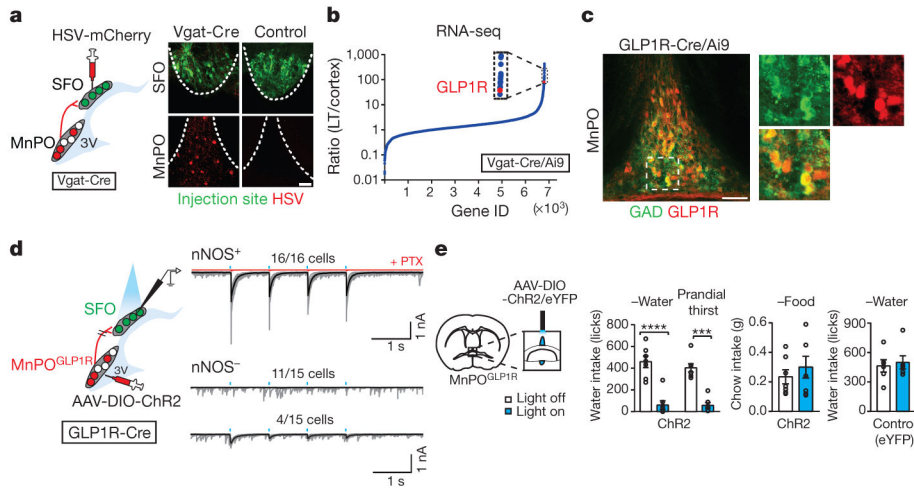
Figure 2 |. GLP1R-expressing GABAergic neurons in the MnPO are a major source of inhibitory input to the SFO.

a, GABAergic input to the SFO. Representative image of the SFO and MnPO after co-injection of AAV-Syn-GCaMP6s (green) and HSV-mCherry (red) in the SFO (one out of four mice). **b**, GLP1R expression is enriched in inhibitory neurons from the lamina terminalis (LT) relative to the cortex. **c**, MnPO^{GLP1R} neurons are GABAergic ($84.7 \pm 3.4\%$ of GAD$^+$ neurons are tdTomato$^+$, $n = 3$ mice, representative images are from one out of three mice). These neurons did not overlap with glutamatergic neurons ($4.3 \pm 0.9\%$ overlap, $n = 3$ mice, Extended Data Fig. 6a). **d**, The MnPO$^{GLP1R} \rightarrow$ SFO monosynaptic connection. MnPO^{GLP1R} neurons send monosynaptic inhibitory input to SFO^{nNOS} neurons. **e**, Optogenetic stimulation of MnPO^{GLP1R} neurons selectively suppresses water intake ($n = 7$ mice for ChR2 and $n = 6$ mice for control). ***$P < 0.001$, ****$P < 0.0001$, by paired two-tailed t-test. All error bars show mean $\pm$ s.e.m. Scale bars, 50 μm.
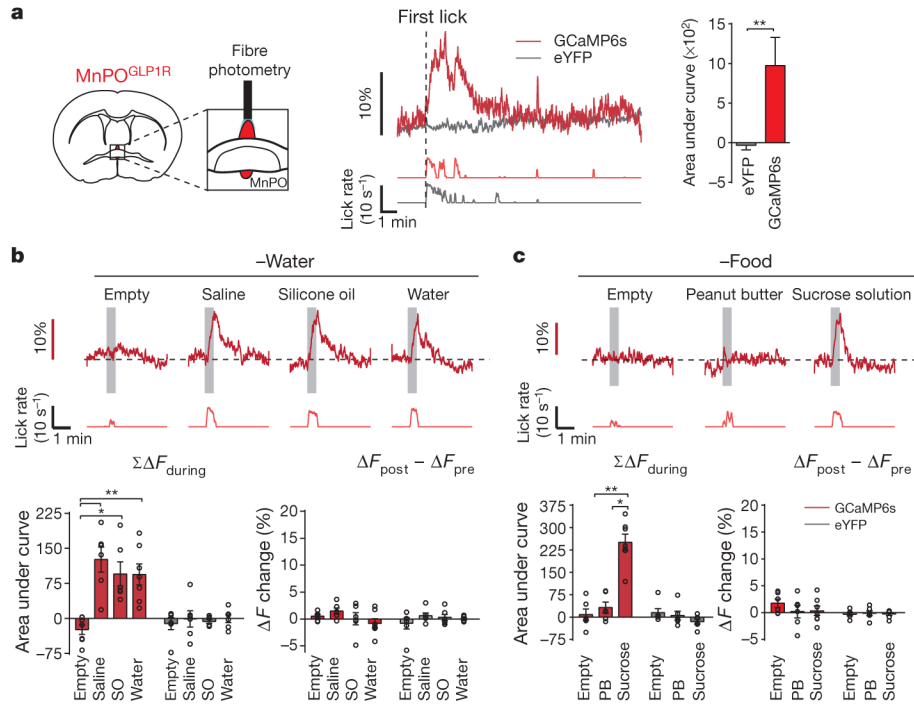
Figure 3 |. Rapid and transient activation of MnPO^GLP1R neurons during drinking behaviour.
a, Fibre photometry recording from MnPO^{GLP1R} neurons (left). MnPO^{GLP1R} neurons are activated upon drinking behaviour (right). Representative traces are from GCaMP6s and enhanced yellow fluorescent protein (eYFP) (one out of six mice). **b**, Responses of MnPO^{GLP1R} neurons under water-restricted conditions towards different types of liquid. Transient activation (bottom left, $\Sigma \Delta F_{during}$) and baseline activity shift (bottom right, $\Delta F_{post} - \Delta F_{pre}$) were quantified ($n = 6$ mice for saline and silicone oil (SO), $n = 7$ mice for empty and water, $n = 6$ mice for all eYFP controls). **c**, Representative responses of MnPO^{GLP1R} neurons under food-restricted conditions. Transient activation (bottom left, $\Sigma \Delta F_{during}$) and baseline activity shift (bottom right, $\Delta F_{post} - \Delta F_{pre}$) were quantified ($n = 6$ mice for empty and peanut butter (PB), $n = 7$ mice for sucrose, $n = 6$ mice for all eYFP controls). *$P < 0.05$, **$P < 0.01$, by two-tailed Mann–Whitney U test or Kruskal–Wallis one-way ANOVA test. All error bars show mean ± s.e.m.
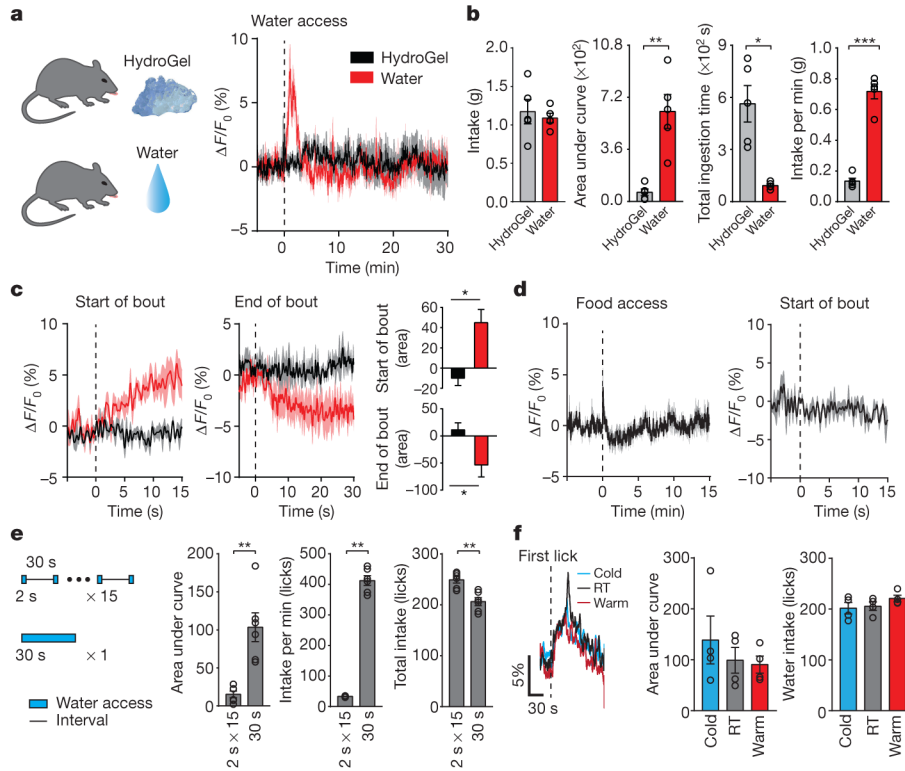
Figure 4 |. MnPO^GLP1R neurons distinguish between drinking and eating behaviour based on ingestive speed.
a, MnPO^GLP1R neurons respond to the intake of liquid water (red) but not HydroGel (black). **b**, Quantification of neural activity and drinking behaviour for the ingestion of HydroGel or water ($n = 5$ mice). **c**, Peristimulus time histogram around the start (left) and the end (middle) of water and gel intake ($n = 5$ mice); quantified data are shown on the right, **d**, Eating solid chow does not stimulate MnPO^GLP1R neurons ($n = 5$ mice). **e**, MnPO^GLP1R neurons are stimulated to a greater extent during periods of concentrated drinking compared with sparse drinking ($n = 6$ mice). **f**, The temperature of the ingested fluid has no effect on MnPO^GLP1R activity. Total responses (middle) and the number of licks (right) were quantified ($n = 4$ mice). $*P < 0.05$, $**P < 0.01$, $***P < 0.001$, by two-tailed Mann–Whitney U test or paired two-tailed t-test. All error bars and shaded areas show mean ± s.e.m.
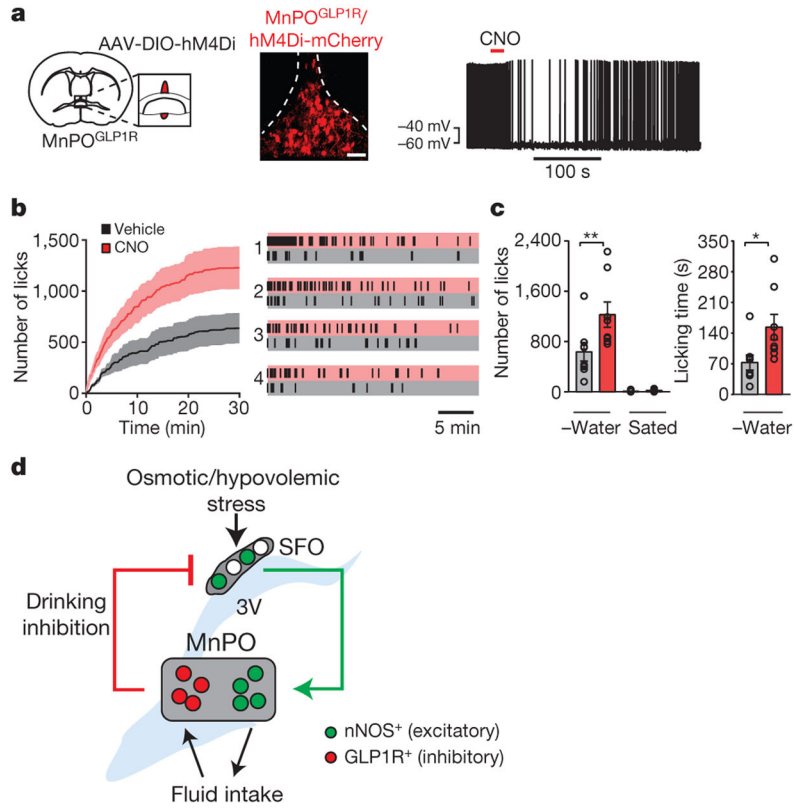
Figure 5 |. Inhibition of MnPO^GLP1R neurons leads to overdrinking.

a, Treatment with CNO inhibits firing in hM4Di-expressing MnPO^{GLP1R} neurons (right, 6 out of 7 neurons). **b**, Acute inhibition of MnPO^{GLP1R} neurons by CNO results in the overdrinking of isotonic saline in water-restricted mice ($n = 8$ mice). Representative lick patterns from four out of eight mice are shown (right). **c**, The total amount of saline intake and the time spent drinking ($n = 8$ mice). **d**, A schematic summarizing thirst genesis, detection of fluid intake and drinking-induced feedback inhibition in the lamina terminalis circuit. $*P < 0.05$, $**P < 0.01$, by paired two-tailed t-test. All error bars and shaded areas show mean ± s.e.m. Scale bar, 50 µm.